Development and Fabrication of Thermally Conductive Polymer Matrix Composite Foams

Hao Ding

A THESIS SUBMITTED TO THE FACULTY OF GRADUATE STUDIES

IN PARTIAL FULFILLMENT OF THE REQUIREMENTS

FOR THE DEGREE OF

MASTER OF SCIENCE

Graduate Program in

Earth and Space Science

York University

Toronto, Ontario

December 2015

ABSTRACT

Advancements in the electronics industry have led to miniaturized components with increased computing power, which resulted in serious heat management issue. Under such technological trend, the development of new multifunctional packaging materials with excellent thermal conductivity and electrical resistivity, which can be used for heat dissipation, is becoming increasingly important. A recent research revealed the possibility of using foaming-induced filler alignment to promote the effective thermal conductivity (k_{eff}). In this context, this thesis research aims to develop thermally conductive polymer matrix composite (PMC) foams that can provide a solution to the heat management of new electronic devices. First, an analytical model was constructed to confirm the feasibility of foaming-induced k_{eff} enhancement. This model considered filler alignment caused by foaming-induced stress field, and calculated the k_{eff} using the concept of thermal resistor network. Second, a comprehensive experimental study was conducted to parametrically reveal the dependency of PMC's k_{eff} on foam morphological parameters, including filler size, foam expansion ratio, cell size, and cell population density. Low density polyethylene (LDPE)-hexagonal boron nitride (hBN) composites blown by Expancel® microspheres were studied as a case example to prove the concept. This study successfully fabricated thermally conductive PMC foams with k_{eff} higher than their solid counterparts, which is the first time reported in the literature. In particular, the k_{eff} of PMC foams filled with 9.21 vol% of hBN_{AC6041} (i.e., submicron-scale) or hBN_{PT110} (i.e., micron-scale) reached as high as 1.16 $W \cdot m^{-1} \cdot K^{-1}$ and 0.97 $W \cdot m^{-1} \cdot K^{-1}$, respectively. These values represented 26% and 21% increases over those of their solid counterparts. Finally, physical foaming was

investigated as a processing method to fabricate PMC foams by using carbon dioxide as the physical blowing agent. The study of physical foaming aims to investigate the possibility of producing thermally conductive PMC foams in a more cost-effective way. Due to the small cell size, no foamed sample demonstrated k_{eff} higher than solid counterpart. However, the k_{eff} was not significantly compromised, while the mass density and material cost were reduced.

ACKNOWLEDGEMENTS

First and foremost, I want to express my sincere gratitude to my supervisor, Professor Siu N. Leung, for his patient guidance, constructive suggestions and the immeasurable amount of support throughout this study. My experience at M^3 Lab has been beneficial to both my research and my professional development.

I would like to extend my appreciation to my committee member, Professor Pouya Rezai, for his meticulous suggestions during the committee meetings.

I would also like to express my thanks to my colleagues and friends at the Department of Mechanical Engineering. I would like to especially thank Dr. Yanting Guo, for her advices and help in my project. My gratitude also goes to Weiqing Fang, Jacob Leung, Ramtin Ardeshiri, Vikash Kumar, and Prateek Jindal. My graduate study has been a wonderful experience with your accompany.

Finally, I would express a deep sense of gratitude to my family. I would like to thank my parents for bringing me to this wonderful world, and always support my decisions. I would also like to thank my wife for her continuous support with unconditional love. It is her encouragement helped me go through the most difficult days.

Table of Contents

List of Tables

List of Figures

Chapter 1

Preamble

1.1 Introduction

Transistor density on an integrated circuit has increased rapidly in the past fifty years [1]. By virtue of the emerging three-dimensional (3-D) chip architecture, this trend is expected to continue for at least another decade [2]. Such technological advancement enabled the fabrication of powerful and miniaturized processors. However, the improved performances of components with smaller footprints brought dramatic increase in heat density. In order to avoid the hardware failure caused by excessive heat accumulation, new techniques for faster heat dissipation are in great demand.

Traditionally, most electronic devices' heat management relied on embedded metallic (mostly aluminum) heat sinks [3, 4]. However, the metallic heat sinks are electrically conductive. As a result, a layer of electrically insulating packaging material is required to separate the heat sink and the circuit board. Currently, Kapton® is the common material used for such electrical insulation layers. However, its low thermal conductivity (0.12 W/m·K at room temperature) limited the heat dissipation rate [5]. Moreover, the metallic heat sinks are heavy, costly, and have difficulties to be incorporated in thin packages [3]. If the new material has a good thermal

conductivity, it is possible to incorporate the heat dissipation into the packaging, which would be beneficial in terms of reducing the weight and size of the device.

For materials used in electronic packaging applications, the properties of high thermal conductivity and good electrical resistivity are necessary. Thermally conductive materials can allow the heat generated within the device to be transferred to the surface and dissipate. High electrical resistivity can eliminate the current leakage, thus prevent circuit failure resulted from current loss [6]. The ideal material should also have a thermal expansion coefficient close the surrounding materials, so that thermal mismatches can be minimized [7]. Moreover, the material should have good processability, so that it can be easily fabricated into complex geometries to fulfill the need. Due to the miniaturization of electronic devices, light weight is also a desirable property. Finally, lower cost is always appreciated in the industry.

In search of the superior electrical insulating property, low cost, light weight, and good processability, polymers, such as epoxy, have been widely used as traditional integrated circuit packaging materials [8]. However, their low thermal conductivities resulted in unsatisfactory performance in dissipating heat for new electronic devices. Therefore, the development of new thermally conductive polymer matrix composites (PMC) without compromising the aforementioned benefits of polymers would be welcomed by electronics manufacturers in order to partially resolve the challenges of heat management in the next generation powerful microelectronic devices. In this context, active research has been conducted to design thermally conductive PMCs by embedding thermally conductive fillers (e.g., metals [9, 10], ceramics [11, 12], and carbon-based fillers [13, 14]) into polymer matrices.

Research has been conducted with numerous polymer matrices, filler materials, as well as fabrication methods [9 - 14]. When the filler content is restricted to 33 vol.%, the effective thermal conductivity (k_{eff}) of the PMC can only reach approximately 2.5 $W \cdot m^{-1} \cdot K^{-1}$, by utilizing hybrid fillers to promote the formation of thermally conductive network [12]. Although the k_{eff} can be further increased by using higher filler content, this approach could compromise some of the key benefits of polymer based materials. The viscosity of the molten composite increases with increasing filler content, making the material more difficult to process. Although such increased viscosity depends on the size, shape, aspect ratio, and ultimately the packing factor of the filler material [15], studies have suggested that filler loading should be less than 40 vol.% in order to maintain the ease of processing [16, 17]. Therefore, it is required to develop new strategies to promote the k_{eff} with low filler content.

In a recent study, Chen *et al.* demonstrated that foaming-assisted networking of hBN in linear low density polyethylene composites would help to fabricate novel light-weight thermally conductive PMC [18]. Although PMC foams with k_{eff} higher than their solid counterparts could not be achieved, it has revealed a new direction to design and fabricate thermally conductive polymer based material system. The authors believed the unexpected high k_{eff} was attributed to foaming-induced filler alignment around expanding air bubbles, but the underlying mechanisms still need to be revealed. In this context, this thesis research aimed to explore the governing factors of PMC foam's k_{eff}, and to identify strategies to fabricate PMC foams with further enhanced k_{eff}.

1.2 Research Goal and Objectives

The focus of this thesis is to develop thermally conductive PMC foams that can be used for heat management applications of future microelectronic devices. In addition to good thermal conductivity, such PMC foams should be combined with outstanding electric insulation, tailored mechanical properties, as well as good processability. To achieve the ultimate goal, the following objectives are proposed: 1) confirm the feasibility of foaming-induced k_{eff} enhancement by developing an analytical model to simulate the PMC foam's k_{eff}; 2) investigate the structure-to-property relationship of thermally conductive PMC foam parametrically and identify strategies to promote the PMC foam's k_{eff} with a comprehensive experimental study; and 3) explore the possibility of industrial viable production by studying physical foaming process to fabricate thermally conductive PMC foams.

1.3 Thesis Structure

This thesis contains six chapters. As an introduction, Chapter 1 identifies the demand of thermally conductive PMC with low filler loading and good electrical resistivity, as well as outlined the goals and objectives of this research. Chapter 2 provides essential background information and a literature survey of related previous researches. The body of this thesis (Chapter 3, 4 and 5) present three research sub-phases. In Chapter 3, an analytical model was developed to confirm the feasibility of foaming-induced k_{eff} enhancement. After being verified with existing experimental data, this model was used to explore the dependence of k_{eff} on their foam morphology. Chapter 4 presented a comprehensive experimental study that reveals the

dependence of k_{eff} on foam morphology. Strategies of using foaming to promote k_{eff} have been identified. Chapter 5 explores the feasibility of producing thermally conductive PMC foams with a physical foaming process. Although no foamed samples demonstrated k_{eff} higher than the solid counterpart, the k_{eff} of samples with 35% volume expansion was found to be comparable to the solid composite. In other words, the mass density and material cost were reduced without significantly compromise the k_{eff}. Finally, Chapter 6 concludes the thesis research. It provides an overview of the contribution of this research and recommendations for future work.

Chapter 2

Background and Literature Review

2.1 Thermal Conductivity and Heat Transfer

Heat transfer is the exchange of thermal energy due to temperature difference [19]. There are three mechanisms of heat transfer: conduction, convection, and radiation. For solid material, the main mechanism is heat conduction, which is governed by Fourier's law of heat transfer (Equation 2.1) [20].

$$\dot{q} = -k \cdot \nabla T \tag{2.1}$$

where $\dot{q}$ is the heat, k is the thermal conductivity of the material, and ∇T is the temperature gradient along the heat transfer direction.

Equation 2.1 suggests that the rate of heat transfer is proportionally related to the temperature gradient and the thermal conductivity. The thermal conductivity of a material is the macroscopic property with different methods of transferring heat summed up. In solid materials, there are two main methods of heat transfer: 1) free electron transport; and 2) phonon transport [21]. While electron transport is the major mechanism in metallic materials [22]; the dominating heat transfer mechanism in dielectric materials (e.g., polymers, and ceramics) is phonon transport, due to the lack of free electrons [23]. Since materials with free

electrons are typically electrically conductive and cannot be used as electronic packaging, this review only focused on the materials that transfer heat using phonon transport.

Phonons are a collective excitation in a periodic and elastic arrangement of atoms or molecules [24]. A perfect crystal can be visualized as a collection of ordered atoms connected by springs [25]. The transfer of heat can be simplistically envisioned by transferring the kinetic energy of one or more vibrating atoms to other atoms. The kinetic energy would propagate through the atoms in manner similar to phonon transport. The effectiveness of phonon transport is limited by the scattering of phonons as they propagate through the atoms, which is greatly affected by the material structure.

For polymers, the inherent lack of free electron makes phonon transport the predominate method of heat transfer. However, the large degree of phonon scattering lead to very low thermal conductivity (typically between 0.1 to 0.3 $W \cdot m^{-1} \cdot K^{-1}$), due to the presence of defects such as polymer chain ends, entanglement, random orientation, voids and impurities, etc [26]. Once these defects are eliminated, researches have shown that single polymer chain or nano-sized polymer fiber can reach a one-dimensional thermal conductivity greater than 100 $W \cdot m^{-1} \cdot K^{-1}$ [27, 28].

Ceramics is another class of dielectric material, which also relies on phonon transport for heat transfer. Although heat transfer by phonon transport is not as efficient as that by free electrons, some ceramic materials exhibit high thermal conductivity. Such ceramic materials have the structural properties (i.e., low atomic mass, strong interatomic bonding, and simple

crystal structures) that can reduce the degree of phonon scattering [29-31]. Such ceramics can be ideal material as thermally conductive fillers to promote the k_{eff} of PMCs.

2.2 Thermally Conductive PMCs

2.2.1 Composite Materials

A composite material is a material made from two or more constituent materials with significantly different physical and/or chemical properties that, when combined, produce a material with characteristics different from the individual components [32]. This research focuses on thermally conductive PMCs, which consist of polymer matrices and thermally conductive fillers.

2.2.1.1 Polymer Matrices

Polymers are extremely long chained molecules that have repeating units (monomers). The long molecular chains are usually entangled so that the relative movement of each molecule is restricted, and the stable shape can be achieved [33 - 35]. Researches have shown that the entanglements are critical to the viscoelastic, melt viscosity, and mechanical properties of the polymer [33, 36].

Many polymers are amorphous, meaning that they do not exhibit any crystalline structures. In an amorphous polymer, the molecules are oriented randomly and intertwined. In general, amorphous polymers have good mechanical properties, uniform thermal expansion, as well as being transparent [34].

In contrast, semi-crystalline polymers have some crystalline regions, normally orient themselves in a lamellae structure [33]. Semi-crystalline polymers generally have anisotropic shrinkage during cooling and good chemically resistance to some extreme environments [34].

In terms of thermal conductivity, it has been experimentally shown that increase in crystallinity led to increased thermal conductivity [37, 38]. It was also found that semi-crystalline polymer composites are more thermally conductive than their amorphous counterparts at the same loading of fillers [39].

2.2.1.2 Thermally Conductive Fillers

Thermally conductive fillers can be categorized by their material type, size, as well as geometry. Commonly used fillers are metals, ceramics and carbon-based materials in both micron and nano size [9 - 14]. In terms of the geometry, fillers can be categorized as 1-dimensional (1D), 2-dimensional (2D) and 3-dimensional (3D) fillers. 1D fillers have a structure that is long in one dimension, while the other two dimensions are very small compared to the length. An example of 1D filler would be carbon nanotubes (CNTs). 2D fillers normally have a layered structure, whose thicknesses are insignificant when compared with their lateral sizes. Common 2D fillers include graphene, and hexagonal boron nitride (hBN). 3D fillers have similar sizes in all dimensions, such as carbon black and cubic boron nitride (cBN).

Unlike metals and carbon-based materials, ceramics are inherent electrical insulators, making them ideal fillers for thermally conductive PMCs in electronic packaging industry. Owing to the diverse crystal structures, ceramics have a very wide range of thermal conductivity. In

general, ceramics with strong interatomic bonding and simple crystal structures normally have relatively high thermal conductivity [30]. For instance, fine aluminium nitride has been reported to have a thermal conductivity of 220 $W \cdot m^{-1} \cdot K^{-1}$ [40]. Depending on the crystal structure, ceramics can also have anisotropic thermal conductive property. For example, hexagonal boron nitride (hBN) has a graphite-like 2D structure. Within each layer, boron and nitrogen atoms are connected by strong covalent bounds, whereas the layers are held together by weak van der Waals forces. The values of over 300 $W \cdot m^{-1} \cdot K^{-1}$ in-plane thermal conductivity and 3 $W \cdot m^{-1} \cdot K^{-1}$ through-layer thermal conductivity are reported for hBN [41]. The anisotropic thermal conductivity provided the feasibility of designing thermally conductive PMCs by tailoring the alignment of isotropic ceramic fillers.

2.2.2 Fabrication Methods of Polymer Composites

In order to disperse fillers into the matrix material, different mixing techniques have been studied, such as powder mixing [42], solution mixing [43], roll milling [44], melt compounding [45], and in situ polymerization [46]. Powder mixing disperses fillers with dry-blending method, in which polymer matrix and filler powders are mixed by continuous tumbling action at room temperature. In solution mixing, polymer matrix and filler materials are first dispersed and mixed in a solvent (e.g. water, toluene, and ethanol); and the solvent was then removed (i.e., evaporated at room or elevated temperature). Roll milling mechanically knead filler particles into melted polymer matrix. Melt compounding disperses the filler into polymer matrix using a twin-screw compounder to combine them while the polymer is in a molten state.

For in situ polymerization, the filler particles are dispersed with the monomers of the matrix material in a solution, in which the polymerization will take place.

In order to compare the fabrication process's effect on the PMC's k_{eff}, Agari *et al*. tested the k_{eff} of composites with same composition but fabricated with four different common methods: powder mixing, roll milling, solution mixing and melt mixing [47]. It was found that specimen prepared with powder mixing lead to the highest k_{eff} with same composition. Such results suggested that a non-uniform composite morphology can encourage the formation of conductive networks through the material, hence promote the k_{eff}.

2.2.3 Previous Work on Thermally Conductive PMCs

Thermally conductive polymer matrix composites (PMCs) are often fabricated by adding thermally conductive fillers to polymer matrix. Based on the filler size, PMCs can be divided into two categories: micro-composite and nano-composite. Micro-composites consist of a polymer matrix and micron-sized fillers with particle sizes between 1 and 100 μm. On the other hand, nano-composites are composite materials with fillers in nanometer scale in at least one dimension, typically less than 100 nm [32]. Both micro-composite and nano-composite have been extensively studied to achieved enhanced the k_{eff}. Previous efforts can be categorized into three major approaches: (1) incorporation of fillers with higher thermal conductivities; (2) promoting the formation of filler network; and (3) increasing filler-polymer compatibility.

2.2.3.1 Incorporation of Fillers with Higher Thermal Conductivities

The most commonly used PMCs in electrical packaging industry are silica-filled epoxy composites called epoxy molding compounds (EMCs). The EMCs have been used widely as the electronic packaging material since 1970s, due to the good mechanical properties and low cost [48]. With the advances in nano-science and nano-technology, researches have been conducted on epoxy/silica nano-composites to further promote the k_{eff} of the composite, and increase the heat dissipation rate [49, 50].

However, silica has a low thermal conductivity of 1.5 $W \cdot m^{-1} \cdot K^{-1}$, which limited the achievable k_{eff} of silica-filled PMCs. In order to further increase the thermal conductivity, researches have been conducted with more thermally conductive ceramic fillers, such as aluminum nitride (AlN) [51], alumina (Al_2O_3) [52], zinc oxide (ZnO) [53], and hexagonal boron nitride (hBN) [54]. Adding 50 vol.% of AlN increased the thermal conductivity 10 times compared to pure polymer [49], while silica-filled epoxy with same filler volume fraction only increased the k_{eff} by two times [48]. However, the application of AlN/polymer composite is restricted by the processing difficulties caused by the high hardness of AlN [41]. Similarly, AlN, Al_2O_3 and ZnO are also extremely abrasive and can possibly damage extrusion and moulding equipment during processing [41]. By contrast, hBN is much softer, hence hBN filled PMCs have much better processibility when same volume fraction of filler is loaded [41]. Moreover, hBN can be processed to thin flakes, because of its graphite-like two-dimensional structure. This provided the possibility to create interconnected conductive filler network with lower filler content. The anisotropic thermal conductivity of hBN also made it feasible to increase the PMCs'

k_{eff} by aligning the hBN along the heat transfer direction. As a result, hBNs with different sizes and geometries have been studied extensively as thermally conductive fillers [11, 16, 41, 54, 55].

The success in further promoting the k_{eff} of PMCs by replacing silica with hBN demonstrated one method to improve the k_{eff} of PMCs (i.e., the incorporation of fillers with higher thermal conductivity). However, both theoretical and experimental work showed that there is a limitation of this method [24, 56, 57]. Bigg has shown that when the ratio between filler's and polymer matrix's thermal conductivities exceeds 1000, further increase in filler's thermal conductivity has negligible effect on the k_{eff} of composites with randomly dispersed filler [24]. Experimental studies also showed that the inclusion of carbon-based fillers with extremely high intrinsic thermal conductivity (e.g., carbon nanotubes and exfoliated graphite nanoplatelets) in PMC failed to significantly increase PMC's k_{eff} [56, 57]. This limitation has been commonly believed to be attributed to the reliance of heat transfer by phonon transport and the high thermal contact resistance at the filler-polymer and/or filler-filler interfaces [23]. The imperfect connections at these interfaces would lead to significant phonon scattering, and thereby hindering phonon transport [21]. As a result, the PMCs were unable to take full advantage of the fillers' high intrinsic thermal conductivities. To avoid this problem, efforts have been made to promote filler interconnections and to increase filler-polymer compatibility.

2.2.3.2 Promoting the Formation of Thermally Conductive Filler Chains

In previous experimental studies, a non-linear relationship was typically found between the filler loading and composite's k_{eff} [51-55]. This phenomenon is believed to be attributed to the interaction between the filler particles, forming conductive paths in the direction of heat

transfer and lead to increased thermal conductivity [55]. In an attempt to develop a predictive model for the k_{eff} of two-phase composite, Agari and Uno studied the probability of forming conductive particle chains with respect to different filler concentrations [58]. It was found that, (1) the amount of formed conductive chains increased exponentially with increase of content of filler particles; and (2) the conductive chains could largely increase thermal conductivity of the composite [58].

The idea of promoting PMC's k_{eff} by forming more conductive filler chains has led to three research approaches: (1) tailoring micro-and-nano structure during fabrication process, (2) using fillers with higher aspect ratio, and (3) incorporate hybrid fillers with different sizes and/or geometries.

In order to tailor the micro-and-nano structure, electric field-induced filler alignment [59], ultra-drawing [60], ultra-sonication [61], and foaming [62], have been studied. Using electric field to align multi-wall carbon nanotubes (MWCNT) in epoxy resin, Martin *et al.* obtained composites that were suitable for electrostatic dissipation [59]. The observed orientation of the field-induced nanotube networks also showed promising optical transparency. In a study of liquid crystal polymer (LCP)-graphene nanoplatelets (GNP) nanocomposite, Leung *et al.* found that ultra-drawing of LCP-GNP nanocomposite would enhance alignment of LCP fibrils and the embedded GNP, which increases the k_{eff} of the nanocomposite [60]. Yu *el al.* used ultra-sonication to disperse hybrid single wall carbon nanotube (SWCNT) and GNP in epoxy [61]. With the formation of thermally conductive filler network, they were able to fabricate PMC that achieved k_{eff} of 3.35 $W \cdot m^{-1} \cdot K^{-1}$ with only 20 wt%

of filler. Furthermore, Okamoto *el al.* demonstrated that foaming-induced biaxial flow aligned clay particles along the cell boundary in a polypropylene matrix, which would suppress cell rupture [62]. Although some of these studies are aimed to improve mechanical and electrical properties, the evidence of promoting filler networking to promote the k_{eff} of PMCs is promising.

Fillers with high aspect ratio also can promote the formation of conducting networks by lowering the percolation threshold [63]. Although the k_{eff} does not exhibit a percolation behavior, the filler interconnection can diminish the disadvantageous role of interfacial thermal resistance [64, 65]. Kochetov studied the effect of filler size and shape on the k_{eff} of hBN particles dispersed in epoxy resin [66]. This study used hBN spherical agglomerates with diameters of 70 nm and 1500 nm (1.5 μm), as well as platelets with lateral size of 500 nm. It was found that the PMCs filled with same amount of the two spherical agglomerates have their k_{eff} values almost the same; while the PMCs filled with hBN platelets have higher k_{eff} than the PMCs filled with both sized hBN spherical agglomerates. In a different study, Kapadia *et al*. studied the k_{eff} of PMCs filled with MWCNTs with four different aspect ratios (i.e. 35, 70, 140 and 280) [65]. It was found that the k_{eff} of the composite increased by increasing the length of MWCNTs while maintaining the same diameter (i.e. increase the aspect ratio).

Finally, efforts have been made to promote the formation of filler network by using hybrid fillers with different sizes and/or geometries [4, 12, 67]. The SEM images in one of these studies clearly showed that the secondary fillers promoted the interconnection among the primary fillers through the formation of structured network [12]. These researches used different polymer matrix materials, and all reported the k_{eff} of PMCs with hybrid fillers are

higher than the non-hybrid counterpart. In a study by Lee *et al*., various inorganic fillers including aluminum nitride (AlN), wollastonite, silicon carbide whisker (SiC) and boron nitride (BN) with different shapes and sizes were used alone or in combination to prepare thermally conductive epoxy-based composites. It is found that composites containing hybrid spherical and fibrous fillers have enhanced thermal conductivity at low to intermediate filler content [4]. In a different study, Leung *et al*. investigated the polyphenylene sulfide (PPS) based composites with hybrid ceramic and carbon based fillers. The primary fillers are two different grades of hBN (platelets and spherical agglomerates), and the secondary fillers are MWCNTs and carbon fibers (CFs). It was found that there exists an optimal volume ratio between the two fillers to maximize the k_{eff} for each combination of hybrid filler system. Moreover, the experimental results demonstrated secondary fillers with a higher aspect ratio and smaller size (e.g., MWCNT) to be more effective in promoting the composite's thermal conductivity [12]. In a recent study, Mosanenzadeh *et al*. reported PLA based composites with k_{eff} as high as 2.77 $W \cdot m^{-1} \cdot K^{-1}$ with 33.3 vol.% of hybrid hBN and GNP, owning to the enhanced interconnected micron-and-nano thermally conductive networks [67].

2.2.3.2 Increasing Filler-Polymer Compatibility

It is well accepted that phonon scattering can lead to a thermal resistance at particle interfaces, and such resistance value depends on the pair of materials [21, 23, 27]. In a study of polypropylene (PP) based composites, Weidenfeller *et al*. found that the k_{eff} of copper (k = 400 $W \cdot m^{-1} \cdot K^{-1}$) filled composites are lower than that of talc (k = 10.6 $W \cdot m^{-1} \cdot K^{-1}$) filled composites with same filler loading, despite that copper is much more thermally conductive than talc [68].

This is attributed to the fact that copper is less compatible with the PP matrix, hence the interfacial thermal resistance is larger [68]. In order to reduce the interfacial thermal resistance, researches have been conducted to perform surface modifications.

In a study of epoxy-AlN composite, Choudhury *et al*. found that the k_{eff} of silane coupling agent (SCA) modified composites are higher than the unmodified counterparts [69]. Similar, Irwin *et al*. reported polyamide nanocomposites filled with coated nano fibers exhibited a 11% increase in k_{eff} compared to the unmodified counterparts [70]. Rong *et al*. reviewed a large number of researches that attempted to use coupling agents to obtain a better interaction between fillers and matrix [71]. It was concluded that suitable surface modification can reduce the interfacial thermal resistance, which suppress phonon scattering and lead to higher k_{eff}.

2.3 Predictive Thermal Conductivity Models

Determining the k_{eff} of a composite material is an outstanding problem in mathematical physics as well as material science; and has been well studied for over a hundred years. This section will review some of the most popular models in determining the k_{eff} of composite materials, including their benefits, accuracies, assumptions and limitations.

2.3.1 Basic Models

The most basic predictive models are parallel model and series model [72]. Parallel model is based on the standard mixture rule (Equation 2.2); and series model is based on the inverse mixture rule (Equation 2.3). Another basic model is the geometric model, which is based on the geometric mean of matrix and filler thermal conductivity (Equation 2.4) [73].

$$k_{eff} = \sum_{i=1}^{n} \phi_i k_i \tag{2.2}$$

$$k_{eff} = \sum_{i=1}^{n} \frac{\phi_i}{k_i} \tag{2.3}$$

$$k_{eff} = \sum_{i=1}^{n} k_i^{\phi_i} \tag{2.4}$$

where k_{eff} is the effective thermal conductivity of the composite, ϕ is the volume fraction of the constituent, k is the thermal conductivity of the constituent, n is the number of constituents in the composite, and i is the index variable for the constituents.

The parallel model considers a case where the constituents are connected in parallel with respect to the heat transfer direction; while the series model treats all constituents are connected in series along the direction of heat transfer. These two models considered two extreme cases. Generally speaking, the parallel model provides an upper bound of the k_{eff}, and the series model gives a lower bound of the k_{eff}. The geometric model calculates the k_{eff} of composite using a geometric mean of the thermal conductivity and volume fraction of the constituents, and does not have a physical basis.

2.3.2 Advanced Models

The study of heat conduction in composite materials is inherently difficult, due to the fact that it is hard to obtain a clear mathematical description of the complex microstructure. Maxwell's seminal work in 1873 pioneered in the study of the thermal conductivity of two-

phase mixtures [74]. Using the potential theory, Maxwell obtained the k_{eff} of a two-phase mixture consisting of randomly distributed and non-interacting homogeneous spheres in a homogeneous medium. The resulting model can be found in Equation 2.5.

$$k_{eff} = k_p \left(\frac{k_f + 2k_p + 2\phi_f \left(k_f - k_p \right)}{k_f + 2k_p - \phi_f \left(k_f - k_p \right)} \right) \tag{2.5}$$

where k_{eff} is the effective thermal conductivity of the composite, ϕ_f is the volume fraction of the filler, k_f is the thermal conductivity of the filler, and k_p is the thermal conductivity of the polymer matrix.

It should be noted that this model assumed that the particles are sufficiently far apart that the potential around each sphere will not be influenced by the presence of other particles. For composites with low filler loadings, where filler particles are generally not interacted, this model can generate accurate predictions. However, this model is not applicable to composites with high filler content, where filler particles are interconnected to each other [75].

Bruggeman used different permeability and field strength assumptions than Maxwell, and derived a different implicit equation (Equation 2.6) to predict the k_{eff} of two phase composites [76]. Similar to Maxwell model, this model does not capture the filler interaction, and the predictions at high filler loadings are not valid [75].

$$1 - \phi_f = \left(\frac{k_f - k_{eff}}{k_f - k_p} \right) \left(\frac{k_p}{k_{eff}} \right)^{1/3} \tag{2.6}$$

where k_{eff} is the effective thermal conductivity of the composite, ϕ_f is the volume fraction of the filler, k_f is the thermal conductivity of the filler, and k_p is the thermal conductivity of the polymer matrix.

In order to predict the k_{eff} of composites with high filler loadings, Agari *et al*. proposed a new model to capture the filler interaction. This model has been modified and improved through a series of studies, and its final form is shown in Equation 2.7 [47, 58, 77, 78].

$$\log k_{eff} = (1-\phi_f)\log\left(C_1 k_p\right) + \phi_f C_2 \log k_f \tag{2.7}$$

where k_{eff} is the effective thermal conductivity of the composite, ϕ_f is the volume fraction of the filler, k_f is the thermal conductivity of the filler, k_p is the thermal conductivity of the polymer matrix, C_1 and C_2 are two constants need to be determined experimentally.

It can be seen that the k_{eff} of a composite is a combination of filler and matrix material. The constant C_1 provides the information about the filler's influence on the secondary structure of the matrix. Higher C_1 value means the filler has less influence on the matrix material's secondary structure. The value of C_2 indicates the level of filler interconnections. Higher C_2 value represents more filler connections within the composite. Both constants (i.e. C_1 and C_2) are ranged from 0 to 1, and need to be determined experimentally [58].

Lewis and Nielsen modified the Halpin–Tsai equation for elastic moduli of composite materials and adapted it to thermal conductivity of particulate-filled composites (Equation 2.8 through 2.10) [79-81].

$$k_{eff} = k_p \left(\frac{1 + AB\phi_f}{1 - B\phi_f \Psi} \right) \tag{2.8}$$

with

$$B = \frac{\left(k_f / k_p \right) - 1}{\left(k_f / k_p \right) + A} \tag{2.9}$$

$$\Psi = 1 + \left(\frac{1 - \phi_m}{\phi_m^2} \right) \phi_f \tag{2.10}$$

where k_{eff} is the effective thermal conductivity of the composite material, k_f is the thermal conductivity of filler, k_p is the thermal conductivity of polymer matrix, ϕ_f is volume fraction of filler, and ϕ_m is the maximum packing fraction.

This model is advanced in the fact that it takes the geometric aspects of fillers into account, and that it can predict a wide range of filler loadings (from 0 to ϕ_m). It should be noted that this model was originally developed for composite materials' elastic modulus, and then translated to predict the k_{eff}. As a result, the interface thermal resistance is not being considered [81, 82]. The parameter "*A*" is accounted for the geometry of the filler, mainly the aspect ratio. The *A* values for some common filler types are listed in Table 2.1 [24]. The parameter ϕ_m is the maximum packing fraction of the fillers. Some common values for are listed in Table 2.2 [24].

Table 2.1 Values of parameter A for common filer types.

Filler Type	Aspect Ratio	*A* Value
Cubes	1	2
Spheres	1	1.5
Randomly oriented fibers	2	1.58
Randomly oriented fibers	4	20.8
Randomly oriented fibers	6	2.80
Randomly oriented fibers	10	4.93
Randomly oriented fibers	15	8.38
Uniaxially oriented fibers (Fiber oriented in direction of heat flow)	---	2L/D
Uniaxially oriented fibers (Fiber oriented transverse to direction of heat flow)	---	0.5

Table 2.2 Maximum packing fraction of some fillers.

Particle Shape	Packing Order	ϕ_m
Spheres	Hexagonal close	0.7405
Spheres	Face centered cubic	0.7405
Spheres	Body centered cubic	0.60
Spheres	Simple cubic	0.524
Spheres	Random loose	0.601
Spheres	Random close	0.637
Irregular	Random close	~0.637
Fibers	Random	0.52
Fibers	Uniaxial hexagonal close	0.907
Fibers	Uniaxial simple cubic	0.785
Fibers	Uniaxial random	0.82

2.4 Polymer Composite Foams

Polymeric foaming is a technology that involves the generation of porous or cellular structures in plastic materials. Foam morphologies are often characterized by the following parameters: (1) foam expansion, which is measured by the volume expansion ratio, and is defined to be the volumetric ratio of the void to solid unfoamed plastic material; (2) average cell size, which is the average diameter of individual air void; (3) cell population density, which is measured by number of air voids per volume of unfoamed plastic material [83]

Depending on the foam morphology and structure, polymer foams can be categorized in the following ways. First, using the average cell size and cell population density, plastic foams can be classified as: conventional plastic foams, fine-cell plastics and microcellular plastics. Table 2.3 listed the range of average cell sizes and cell population densities for each of above mentioned type [84]. Second, plastic foams can be categorized by their cellular structures: closed-cell foams and open-cell foams. In closed-cell foams, individual cells are completely separated by plastic cells walls. In open-cell foams, pores exist on the cell walls so that adjacent cells are interconnected [83].

Table 2.3 Plastic foam classification based on cell size and cell population density.

	Average Cell Size	**Cell Population Density**
Conventional Plastic Foams	>300 µm	$<10^6$/cc
Fine-Cell Plastics	10-300 µm	10^6-10^9/cc
Microcellular Plastics	0.1-10 µm	10^9-10^{15}/cc

2.4.1 Blowing Agents

The foaming process typically involves the following steps: (1) dissolution of a blowing agent into a plastic matrix; (2) generation of pores or cells by phase separation of the blowing agent from the plastic matrix; and (3) stabilization of the porous or cellular structure. In the first step, plastic foams can be blown with either a chemical blowing agent (CBA) or a physical blowing agent (PBA) [83].

2.4.1.1 Chemical Blowing Agents

CBAs release gases (i.e. N_2, CO_2 etc.) when they are heated above their decomposition temperature. The main advantage of CBAs lies in its ease of use. CBAs can be uniformly distributed into polymer matrix prior to foaming process. It is easy to generate a homogeneous polymer-gas mixture. It can also be used in conventional extrusion or injection molding systems to produce foamed plastics without the need to modify the systems [85].

Depending on their enthalpy changes during the decomposition process, CBAs are divided into two groups: exothermic CBAs and endothermic CBAs. Generally speaking, exothermic most CBAs release N_2 upon decomposition, while endothermic most CBAs generate CO_2 as primary gas. Exothermic CBAs release heat during their decomposition. The excess heat can trigger the decomposition of surrounding CBAs; hence the gas releasing rate is relatively fast. Endothermic CBAs, however, absorb heat during decomposition. Therefore, endothermic CBA decomposition reaction requires additional heat, and usually releases gas slowly [83].

There are two key criterions to select the suitable CBA: an appropriate decomposition temperature; and compatible residue. If the decomposition temperature is too low, gas could be generated prematurely, leading to gas loss and/or premature generation of cells. Conversely, when the decomposition temperature is too high, the CBAs may not be active completely, which might cause non-uniform cell structure and/or limited foam expansion. In some cases, activators are added to a CBA to lower the decomposition temperature in order to get desirable decomposition temperature. For example, zinc oxide can reduce azodicarbonamide's decomposition temperature from 205-215°C to approximately 150°C [85]. The other key factor to choose appropriate CBA is the residue product. The residual product from the decomposition of CBA must be compatible with the foam's application and/or plastic matrix material. For example, CBAs that leave toxic residues cannot be used in food packaging industry.

2.4.1.2 Physical Blowing Agents

By comparison, PBAs are materials that are injected into the polymer system as pressurized gas, liquid or supercritical fluid. Using PBAs has a few obvious disadvantages. First of all, relatively high pressure and/or temperature are often required to accelerate the gas dissolution process. Moreover, conventional extrusion and injection molding systems need to be modified in order to use PBAs. However, PBAs are still commonly used in industries due to its low cost and high effectiveness, especially in producing low-density foams. Traditionally, chlorofluorocarbons (CFCs) were widely used. CFCs were ideal PBA choice, due to the high solubility, low toxicity, non-flammability, good thermal and chemical stability, as well as low cost. Owing to the chemical stability, CFCs can reach up into stratosphere, where they break

down and generate chlorine atoms that destroy the ozone layer [85]. Ultimately, this leads to significant increase in UV-B radiation, which is harmful to most biological systems, including human [86]. As a result, the industry has completely stopped using CFCs by the Montreal Protocol [86]. Hydrochlorofluorocarbons (HCFCs) are less chemically stable than CFCs, and tend to break down before they reach the stratosphere. However, they still have potential damage to the ozone layer. Therefore, they were phased out in Europe for the production of foams in 2004 [87]. In other countries, the use of HCFCs is now being restricted in stages by the Montreal Protocol, and they will be completed phased out in 2020 in developed countries and 2040 in developing countries [86]. Other commonly used PBAs include Hydrofluorocarbons (HFCs) and Hydrocarbons (HCs) [83, 85]. However, HFCs have high cost and global warming potentials, and HCs are flammable. Therefore, neither of them is an ideal PBA. Recent attentions have been conducted on using CO_2 and N_2. In particular, CO_2 will be used in this study, owing to its good plasticization effect that allows foaming at relatively low temperature.

2.4.2 Foaming with Expancel® Microspheres

Expancel® Microspheres are small spheres consist of polymeric shells and encapsulated hydrocarbon gases. Expancel® Microspheres can expand and create porous structure at a certain temperature range, owing to the following two simultaneous phenomena: (1) the pressure of encapsulated gas increases with the increasing of temperature; and (2) the polymeric shells softened to allow the expansion of the microspheres. Depending on the grade of Expancel® Microspheres, the on-set temperature as well as pre- and post- expansion diameter may vary [88]. Expancel® Microspheres has been used as a foaming agent in previous

studies, including the study of thermally conductive PMC foams [18]. Such foaming technique allows precise control of the foam morphologies, hence was employed in this study to elevate each of foam morphological parameters effect on k_{eff} of PMC foams.

2.4.3 Batch Foaming

In addition to using Expancel® Microspheres, batch foaming will also be applied in this thesis research as a method to create foam structure. Batch foaming is one of the most studied processes due to the ease of setup and control [85]. The batch foaming process starts by placing the plastic matrix into a pressure chamber, which is to be saturated with a blowing agent (e.g., CO_2) under ambient temperature. The blowing agent will be dissolved into the plastic matrix during the gas dissolution process. After that, a rapid depressurization and subsequent heating are applied to cause a sudden drop of gas solubility, which generates a thermodynamic instability for cell nucleation. The foam expands as cells nucleate and grow. The plastic sample is cooled afterward to stabilize the foam structure.

One challenge of batch foaming is brought by the low gas diffusion rate into the polymer at ambient temperature. The gas saturation process typically takes very long time, depending on sample thickness. Alternatively, the gas saturation process can be conducted at an elevated temperature to reduce the time required. However, an effective cooling strategy is needed to stabilize the foam after depressurization. Otherwise, cell deterioration can occur which leads to non-uniform cell structure and low volume expansion [85].

Chapter 3

Analytical Modelling of Effective Thermal Conductivity of PMC Foams

Foaming has been reported to be an effective method to align filler particles along the cell boundary, and improve mechanical and electrical properties [62, 89, 90]. Chan *et al.*, pioneered a study to investigate the k_{eff} of PMC foams [18]. Although it has been shown that aligning filler particles with foaming-induced biaxial flow can be a possible approach to enhance the PMC's k_{eff}, no experimental result has shown that the k_{eff} of PMC foam can be higher than that of the solid counterpart with same filler loading. As a result, an analytical model was developed at the initial phase of this thesis research to confirm the feasibility of foaming-induced k_{eff} enhancement. After being verified with existing experimental data, this model was further employed to explore the dependence of keff on their foam morphology.

3.1 Theory and Modelling

3.1.1 Formation of heat transfer elements

The model developed in this thesis treated PMC foams as a collection of individual unit cells. The unit cell structure, which consists of a central air void and surrounding wall, is modeled based on the SEM images of thermally conductive linear low density polyethylene

(LLDPE)-hBN composite foams observed by Chan *et al* [18]. It was reported that the hBN platelets aligned along the wall of the cellular structures, and developed into a three-dimensional hBN network in the LLDPE matrix [18]. Figure 3.1 shows a schematic that illustrates the filler alignment caused by foam expansion as observed by Chan *et al.*. The LLDPE-hBN foam consists of individual air void, with hBN platelets aligned along the void. There are layers with only polymers, layers with both polymers and fillers, as well as layers with polymers, fillers and air void. Therefore, this study modelled the PMC foam's microstructure as a collection of evenly distributed cubic cells with thermally conductive filler network aligned along the walls that separate adjacent cells. A schematic of the physical model is depicted in Figure 3.2.

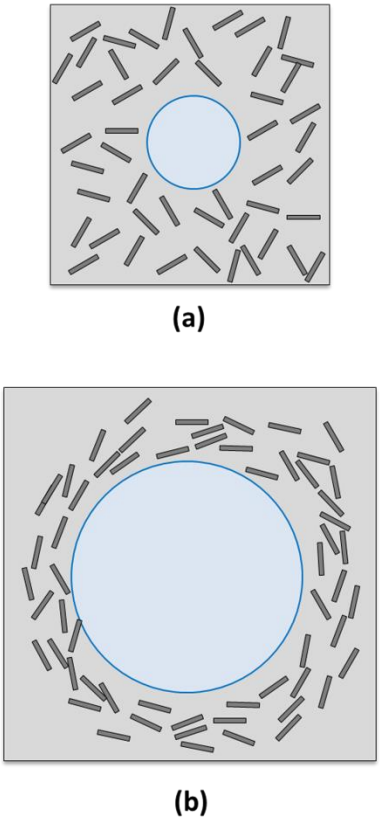

Figure 3.1 Schematics of PMC foam's morphology (a) before significant expansion; and (b) after significant expansion.

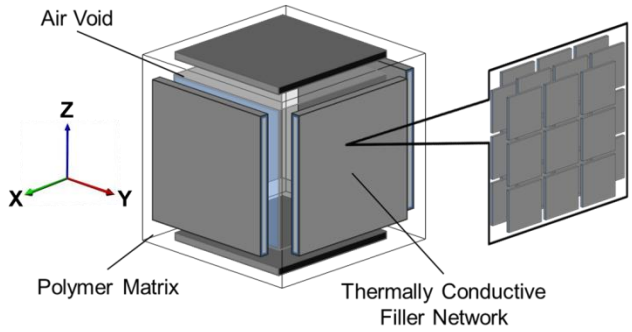

Figure 3.2 A physical model that represents PMC foam's microstructure.

3.1.2 Model Development

Figure 3.3(a) shows the cross-section of the representative volume element (RVE) shown in Figure 3.2. The air void in each RVE is considered to be a cuboid. Considering heat flows along the positive z direction, the polymer matrix, filler platelets, and air void can be represented by a thermal resistor network. Furthermore, it can be mathematically proven that the thermal resistance determined by treating filler platelets shown in Figure 3.3(a) is identical to that determined by treating them as larger clusters as illustrated in Figure 3.3(b). Moreover, a recent research also showed that fillers tend to form agglomerates around air voids [89]. Therefore, the PMC foam's configuration depicted in Figure 3.3(b) has been adopted to develop the analytical model to predict the composite foam's k_{eff}. The four boundary surfaces of the RVE parallel to the heat flow direction are considered to be adiabatic, while the other two surfaces are isothermal with one of them having a higher temperature, namely the bottom surface. Therefore, heat enters the RVE from the bottom boundary surface and exists from the upper boundary surface. Moreover, isotherms are assumed to be perpendicular to the direction of heat flow.

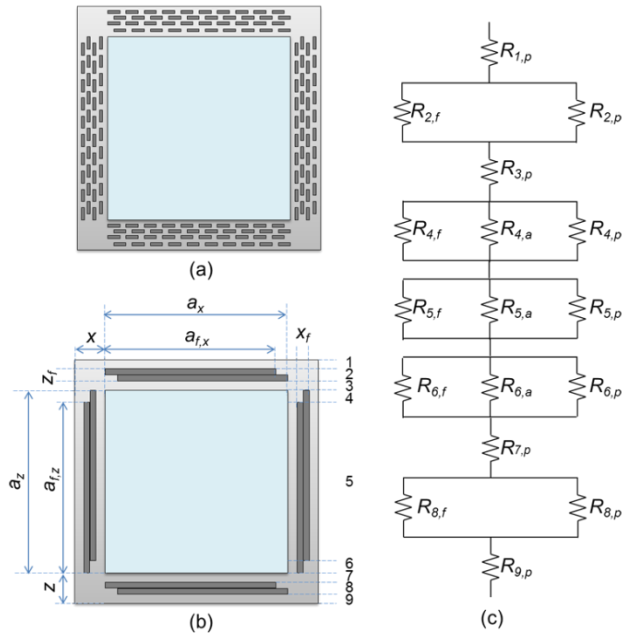

Figure 3.3 (a) Cross-section of the physical model that represents the microstructure of PMC foam; (b) cross-section of the physical model with the consideration of clusters of hBN platelets; (c) a schematic of thermal resistor network that represents the heat transfer element (subscripts *a*, *p* and *f* refers to air, polymer and filler, respectively).

In this model, each RVE consists of 9 groups of thermal resistors connected in series. Their thermal resistances are denoted as R_i, where *i* is the resistor group number ranging from 1 to 9. In each group, thermal resistors of different materials (i.e., polymer, filler, and/or air) are connected in parallel. Figure 3.3(c) illustrates a schematic of the thermal resistor network representing the RVE. The layers consist of only polymer when *i* equals to 1, 3, 7, and 9. For *i* equals to 2 and 8, the layers contain both polymer and filler. Polymer, filler, and air void are coexisting when *i* equals to 4, 5, and 6. The total thermal resistance (R_{total}) is the sum of 9 groups of thermal resistors connected in series, and is given by:

$$R_{total} = \sum_{i=1}^{9} R_i \tag{3.1}$$

According to Fourier's law of heat transfer, the steady state heat conduction through the RVE is given by:

$$\frac{dQ}{dt} = -\frac{k_{eff} A \Delta T}{L_z} = -\frac{k_{eff} \left(a_x + 2x\right)^2 \Delta T}{a_z + 2z} = -\frac{\Delta T}{R_{total}} \tag{3.2}$$

where *dQ/dt* is the rate of heat flow across the RVE; *A* is the cross-sectional area of the RVE perpendicular to the heat flow direction; ΔT is the temperature difference between the top and bottom boundary surfaces; L_z is the length of the heat flow path (i.e., in the z direction); a_x and a_z are the length of the air void in the perpendicular and parallel directions, respectively; and *x* and *z* are the thicknesses of the cell walls parallel and perpendicular, respectively, to the heat flow direction.

Hence, the RVE's k_{eff} can be determined by its total thermal resistance and dimensions by:

$$k_{eff} = \frac{a_z + 2z}{R_{total}\left(a_x + 2x\right)^2} \tag{3.3}$$

The equivalent thermal resistance of the i^{th} layer (i.e., R_i) is expressed as:

$$R_i = \frac{t_i}{k_a A_{i,a} + k_f A_{i,f} + k_p A_{i,p}} \tag{3.4}$$

where t_i is the thickness of the i^{th}layer; k_a, k_f and k_p are the thermal conductivity of air, filler and polymer, respectively; and $A_{i,a}$, $A_{i,p}$ and $A_{i,f}$ represent the cross-sectional area of the air void, polymer and filler, respectively, in the i^{th}layer.

Using Equation (3.4), the equivalent thermal resistance of each layer in the RVE can be derived as Equation (3.5) through (3.8).

$$R_1 = R_3 = R_7 = R_9 = \frac{0.5(z - z_f)}{k_p(a_x + 2x)^2} \tag{3.5}$$

$$R_2 = R_8 = \frac{z_f}{k_p[(a_x + 2x)^2 - a_{f,x}{}^2] + k_f a_{f,x}{}^2} \tag{3.6}$$

$$R_4 = R_6 = \frac{a_z - a_{f,z}}{k_a a_x{}^2 + 2k_f a_{f,x} x_f + k_p[(a_x + 2x)^2 - a_x{}^2 - 2a_{f,x} x_f]} \tag{3.7}$$

$$R_5 = \frac{2a_{f,z} - a_z}{k_a a_x{}^2 + 4k_f a_{f,x} x_f + k_p[(a_x + 2x)^2 - a_x{}^2 - 4a_{f,x} x_f]} \tag{3.8}$$

As shown in Figure 3.3(b), z_f and $a_{f,x}$ are the thickness and length of filler clusters, respectively, in layers 2 and 8; and x_f and $a_{f,x}$ are the thickness and length of filler clusters, respectively, in layers 4 through 6. In these equations, a_x equals to a_z for PMC foams fabricated by isotropic foaming, while they are different for PMC foams prepared by constrained foaming in a preferential direction.

The thermal conductivity of various filler platelets is anisotropic. For example, the in-plane thermal conductivity ($k_{f//}$) and the through-plane thermal conductivity ($k_{f\perp}$) of hBN platelets are 300 $W \cdot m^{-1} \cdot K^{-1}$ and 2 $W \cdot m^{-1} \cdot K^{-1}$, respectively [41, 91, 93]. To account for the

dependence of k_f on the orientation of the thermally conductive filler platelets in the polymer matrix, an alignment factor (α) is introduced in the model as shown in Figure 3.4(a) and (b). In order to describe the same extensional flow field-induced filler alignment in the experimental study of LLDPE-hBN composites foamed by Expancel® microspheres [18], α has been introduced as a function of the volume expansion of the microsphere. Random orientation of hBN platelets in LLDPE matrix can be mathematically approximated by using α equals to 0.5, while α equals to 0 represents perfectly aligned hBN platelets. Assuming the platelets are equally likely to be stacked in a parallel configuration or in a series configuration, k_f can be determined by Equation (3.9) and (3.10).

For i = 2 and 8,

$$k_f = \frac{(\alpha - \alpha^2)k_{f\perp}^2 + 2(\alpha^2 - \alpha + 1)k_{f\perp}k_{f//} + (\alpha - \alpha^2)k_{f//}^2}{2[\alpha k_{\perp} + (1-\alpha)k_{//}]} \tag{3.9}$$

For i = 4, 5, and 6,

$$k_f = \frac{(\alpha - \alpha^2)k_{f\perp}^2 + 2(\alpha^2 - \alpha + 1)k_{f\perp}k_{f//} + (\alpha - \alpha^2)k_{f//}^2}{2[\alpha k_{//} + (1-\alpha)k_{\perp}]} \tag{3.10}$$

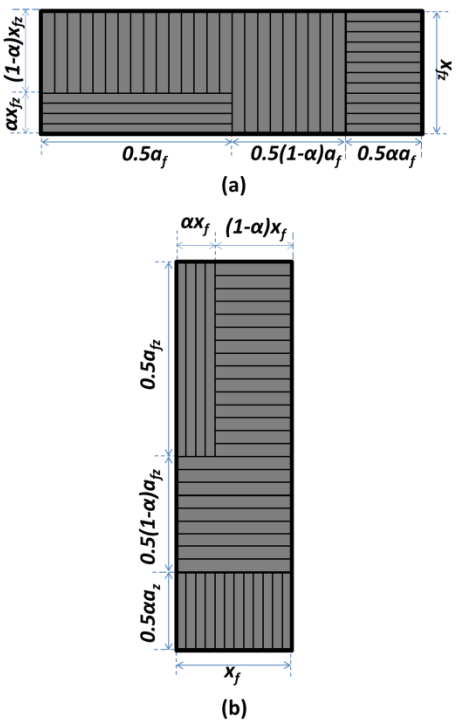

Figure 3.4 Schematics that illustrate the filler orientation in a filler cluster in (a) layers 2 and 8; and (b) layers 4 through 6.

In Equation (3.9) and (3.10), α is a function of expansion of microspheres, and it is expressed as :

$$\alpha = \frac{1}{2}\left(\frac{d_{min}}{d}\right)^3 \tag{3.11}$$

where d_{min} is the edge length of a cubic void that has the same volume as an unexpanded microsphere; $d = a_x$ for layers 2 and 8; and $d = a_z$ for layers 4, 5 and 6.

Using Equation (3.11), α is 0.5 when d equals to d_{min} (i.e., no expansion), suggesting that it is equally likely for the filler platelets to align in the two orthogonal directions. In contrast, α approaches to zero when d approaches to infinity. This is used to model the preferential filler alignment induced by extensional flow fields during foam expansion.

3.2.3 Physical parameters

In this study, LLDPE-hBN foams' k_{eff} was determined using the developed model, and the results were presented as case examples for model validation. The thermal conductivity of LLDPE (k_p), hBN (in-plane) ($k_{f//}$), hBN (through-plane) ($k_{f\perp}$), and air (k_a) used in this work are summarized in Table 3.1 [18, 41, 91, 93].

Table 3.1 Physical parameters used in the calculation of PMC foam's k_{eff}.

	Value	**Unit**
k_p	0.22	$W \cdot m^{-1} \cdot K^{-1}$
$k_{f//}$	300	$W \cdot m^{-1} \cdot K^{-1}$
$k_{f\perp}$	2	$W \cdot m^{-1} \cdot K^{-1}$
k_a	0.024	$W \cdot m^{-1} \cdot K^{-1}$

3.2 Results and Discussion

Considering LLDPE-hBN composite foams as case examples, the k_{eff} of the composite foams calculated using the developed model were compared with the experimental data in literature for model validatation [18]. The cell morphology, including cell size, cell population density, and volume expansion percent specified in the experimental study were considered in these calculations. Consequently, a series of parametric studies were conducted to study the effects of foam morphologies, volume expansion percentages, hBN loadings, and anisotropy of filler's thermal conductivity on PMC foam's k_{eff}. The parametric studies would enhance the elucidation of the structure-to-property (i.e., k_{eff}) relationship of PMC foams.

3.2.1 Effect of foam's volume expansion on PMC foam's k_{eff}

Figure 3.5 plots the calculated k_{eff} for LLDPE-hBN composite foams filled with 50 vol.% hBN as well as the experimental data [18]. Both sets of data showed that k_{eff} decreased initially as the PMC foam expanded. However, once a threshold percentage of volume expansion had achieved, further foam expansion would promote the composite's k_{eff}.

The plot also shows that the calculated k_{eff} were higher than the experimental data. The discrepancy was believed to be caused by ignoring of thermal contact resistance at the interfaces between LLPDE and hBN as well as those between different hBN platelets in the analytical model. Moreover, the in-plane thermal conductivity of hBN might also be lower than the commonly accepted value of 300 $W \cdot m^{-1} \cdot K^{-1}$ [91, 93]. Therefore, the total thermal resistance of the heat transfer element was underestimated and caused the calculated k_{eff} to be higher than the measured value. However, by shifting the calculated k_{eff} downward (i.e., the dash curve in Figure 3.5, which was obtained by subtracting 1.75 $W \cdot m^{-1} \cdot K^{-1}$ from calculated value), it was apparent that the trends had good agreement with the experimental data. This provided evidence that the model developed in this study would offer some insights about the underlying factors that influence composite foams' k_{eff}. To the author's best knowledge, there is no experimental result regarding the thermal contact resistance that applies to this situation. When such value becomes available, the model can further be improved by incorporating the thermal contact resistance.

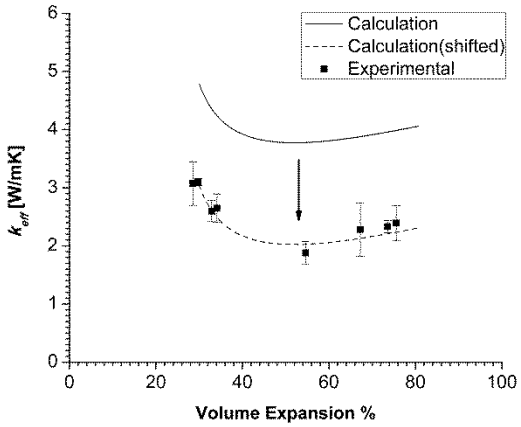

Figure 3.5 Effect of foam's volume expansion on the LLDPE-hBN foam's k_{eff} (The error bars represent one standard deviation of measured data).

Chan *et al.* hypothesized that cell growth would result in two competing effects on the composite foam's k_{eff}: (i) extensional stress-induced hBN alignment along the cell wall would promote the k_{eff}; and (ii) increase in the size of air void would decrease the k_{eff} [18]. As illustrated in Figure 3.6, this hypothesis can be verified by studying the effect of volume expansion on k_{eff} of layer 5 (i.e., the layer with the air void). However, in order to elucidate the effect of foam expansion on the PMC's k_{eff}, it is necessary to analyze its effect on the k_{eff} and volume fraction (Φ_i) for each of the 9 layers in the proposed model.

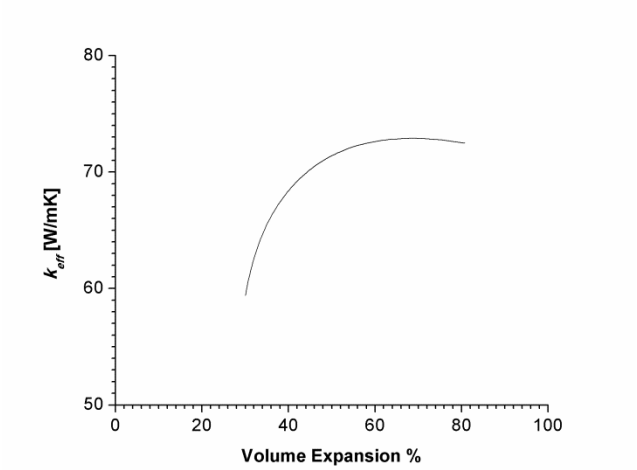

Figure 3.6 Effect of foam's volume expansion on the k_{eff} of layer 5 (i.e., the layer with the air void).

Using Fourier's law of heat transfer, it can be shown that the reciprocal of k_{eff} depends on both Φ_i and the effective thermal conductivity of the i^{th} layer ($k_{eff,i}$) in the thermal resistor network model. Such relationship is shown in Equation (3.12), and the calculated ratios of $\Phi_i/k_{eff,i}$ as well as the reciprocal of k_{eff} are plotted in Figure 3.7.

$$\frac{1}{k_{eff}} = \sum_{i=1}^{9} \frac{\phi_i}{k_{eff,i}} \tag{3.12}$$

It can be observed that the mound-shaped curve for the reciprocal of k_{eff} was predominantly governed by the pure LLDPE layers (i.e., layers 1, 3, 7 and 9) and the layers with hBN preferentially aligned perpendicularly to the heat flow direction (i.e., layers 2 and 8). Figure 3.8 shows that while the thermal conductivity of the pure LLDPE layers were fixed, the volume fraction followed a mound-shaped trend. As illustrated in Figure 3.9, the initial increase of the volume fraction was caused by the reduction in the thickness, and thereby the volume fraction, of the hBN filler clusters in layers 2 and 8. However, as the air void expanded continuously, the volume fraction of the pure LLDPE layers decreased eventually. In layers 2 and 8, the mound-

shaped trend of $\Phi_i/k_{eff,i}$ could be explained by the changes of their k_{eff} and volume fraction during foam expansion, which are shown in Figure 3.9. On the one hand, the reduction of k_{eff} in these two layers as volume expansion percent increased was caused by the preferentially alignment of hBN filler in the direction that was perpendicular to heat flow. On the other hand, the contribution of these layers to the overall k_{eff} of the representative volume element reduced continuously as the volume fraction of these layers decreased with the expansion of the air void. Although layer 5's k_{eff} also followed a mound-shape trend in the range of volume expansion percent considered in this study, the smaller magnitude of $\Phi_i/k_{eff,i}$ in this layer (i.e., the layer with the air void) made its effect less significant than layers 1 through 3 and 7 through 9.

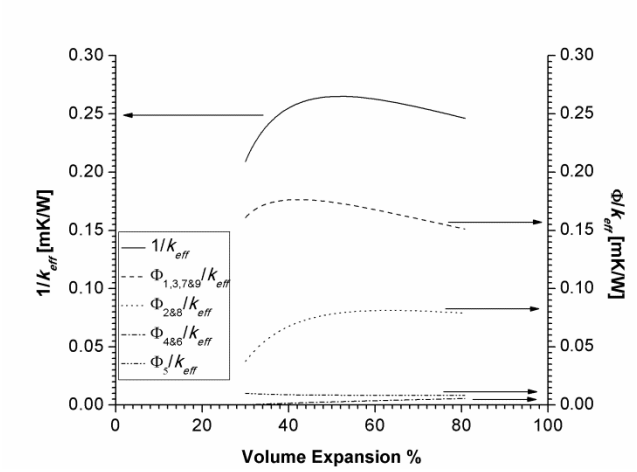

Figure 3.7 Effect of foam's volume expansion on the $\Phi_i/k_{eff,i}$ and $1/k_{eff}$.

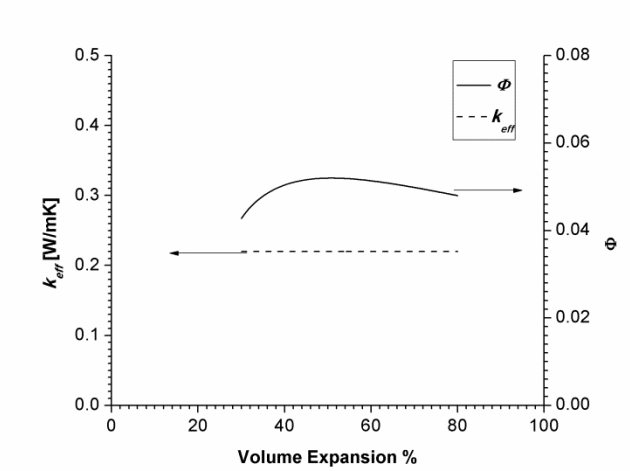

Figure 3.8 Effect of foam's volume expansion on the *Φ and* k_{eff} of pure LLDPE layers.

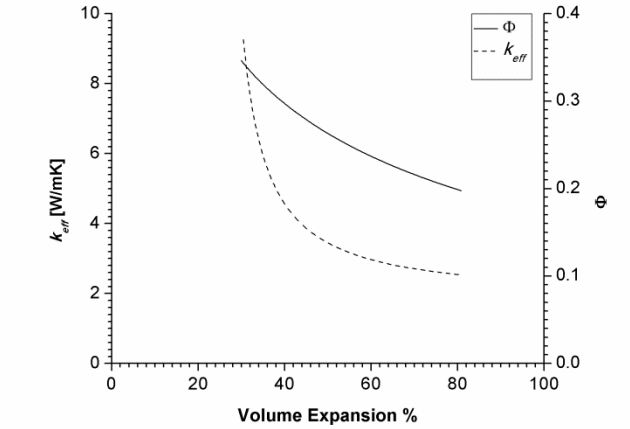

Figure 3.9 Effect of foam's volume expansion on the *Φ and* k_{eff} of layers 2 and 8.

3.2.2 Effect of filler content on PMC foam's k_{eff}

The effect of filler content on PMC foam's k_{eff} is shown in Figure 3.10. The $k_{f//}$ was set to be 300 $W \cdot m^{-1} \cdot K^{-1}$ in these calculations. Apparently, the PMC foams' k_{eff} increased with hBN contents. Moreover, in the absence of hBN filler, LLDPE foam's k_{eff} decreased as the percentage of volume expansion increased. Most importantly, it was found that the threshold percentage of volume expansion (i.e., the volume expansion percent over which the PMC foam's k_{eff} started to increase with further foam expansion) increased with hBN contents. This trend was

consistent with experimental data reported in literature [92].

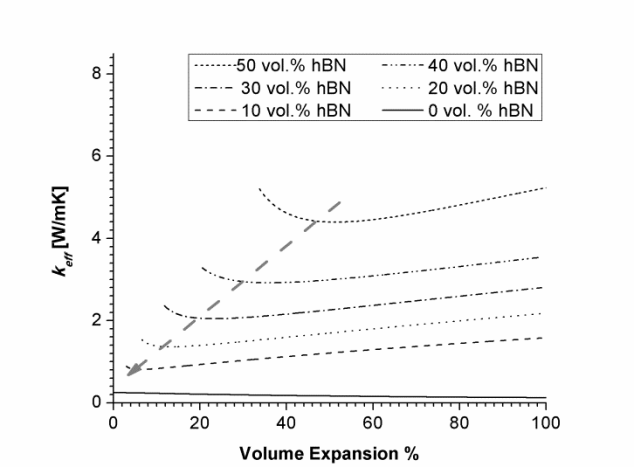

Figure 3.10 Effect of the LLDPE-hBN foam's percentage of volume expansion on its k_{eff}.

The observed structure-to-property relationship, both theoretically and experimentally, revealed that foaming would be a feasible approach to promote PMC's k_{eff}. This is especially beneficial for the PMCs with low filler loadings, which is required to ensure good processability of the material systems. The possibility of increasing PMC's k_{eff} without the need to add a large amount of thermally conductive filler, together with the introduction of cellular structures into the PMC, would ensure low density and good processability. Furthermore, the reduced material consumption would foster the environmental sustainability of the end-products.

3.2.3 Effect of foam morphology on PMC foam's k_{eff}

In order to maintain good processability of polymeric materials, it is beneficial to achieve high PMC foam's k_{eff} with minimal filler loading. In this context, the effects of cellular morphology, including cell size and cell population density, on the k_{eff} of PMC foam filled with low hBN content (i.e., 10 vol.%) were studied using the developed model. Figure 3.11 illustrates the effect of cell size on the PMC foams' k_{eff} with different volume expansion percents. The

calculated results revealed that there was an optimal cell size to maximize the PMC foam's k_{eff}. The optimal cell size increased with the foam's volume expansion percent. Furthermore, the results indicate that PMC foam's k_{eff} increased with volume expansion for the range being considered (i.e., 25% to 200%). This observation was consistent with the results shown in Figure 3.10 (i.e., LLDPE-hBN foams filled with 10 vol.% of hBN). In conclusion, it can be deduced that highly expanded PMC foams by using optimal cell size and introducing high cell population density would be an effective way to promote the composite foams' k_{eff}. This finding helps to guide the design of light-weight thermally conductive PMC foams.

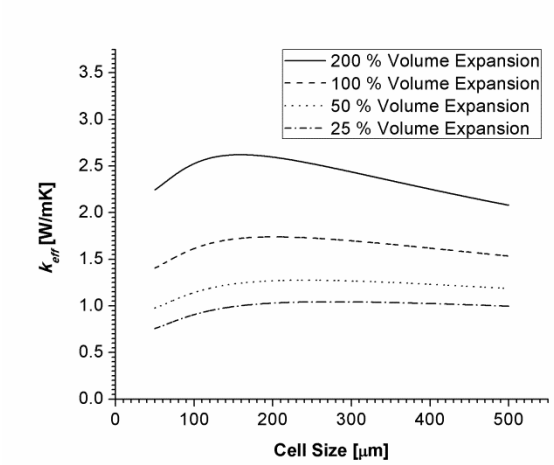

Figure 3.11 Effect of cell size on LLDPE-hBN foam's k_{eff} (note: hBN vol.% = 10 vol.%).

3.2.4 Effect of constrained foaming on PMC foam's k_{eff}

In order to further promote the k_{eff} of PMC foams with low hBN loadings, the effect of constrained foaming (i.e., constrained the foam expansion such that it expands anisotropically in a preferential direction) on PMC foam's k_{eff} was studied by the model. Figure 3.12 shows the influence of a_z/a_x (denoted the elongated ratio in the heat flow direction), ranging from 1 to 10,

on the k_{eff} of LLDPE composite foam with 10 vol.% of hBN. The results revealed that anisotropic foam expansion with $a_z/a_x > 1$ would enhance the PMC foams' k_{eff}.

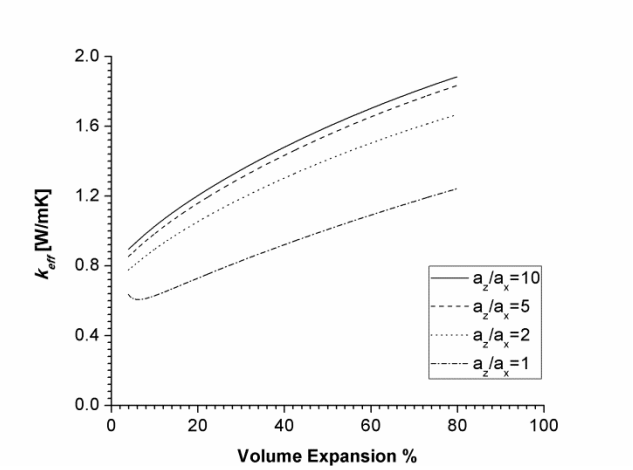

Figure 3.12 Effect of constrained foaming on LLDPE-hBN foam's k_{eff} (note: hBN vol.% = 10 vol.%).

To understand the effects of constrained foaming's enhancement on PMC foams' k_{eff}, Figure 3.13 compared $\Phi_i/k_{eff,i}$ as well as the reciprocal of k_{eff} for LLDPE-hBN composite foams filled with 10 vol.% hBN prepared by both isotropic foaming and constrained foaming with a_z/a_x equaled to 10. Similar to previous discussion regarding the PMC foams filled with 50 vol.% hBN, the reciprocal of k_{eff} could be explained by the pure LLDPE layers (i.e. layers 1, 3, 7 and 9). However, with lower hBN content, the effects of layers 2 and 8 on k_{eff} became insignificant. Therefore, the mound-shaped curves for reciprocal of k_{eff} were predominantly governed by the change in volume fraction of pure LLDPE layers. In the PMC foam based on constrained foaming, the layers with air void (i.e. layer 4, 5 and 6) were longer than those in the PMC foam based on isotropic foaming. In other words, the total volume fraction of these layers was larger, leading to smaller volume fraction of the low thermally conductive pure LLDPE layers. Together with the constant thermal conductivity in the pure LLDPE layers, constrained foaming helped to reduce these layers' $\Phi_i/k_{eff,I}$, and thereby the PMC foam's k_{eff}.

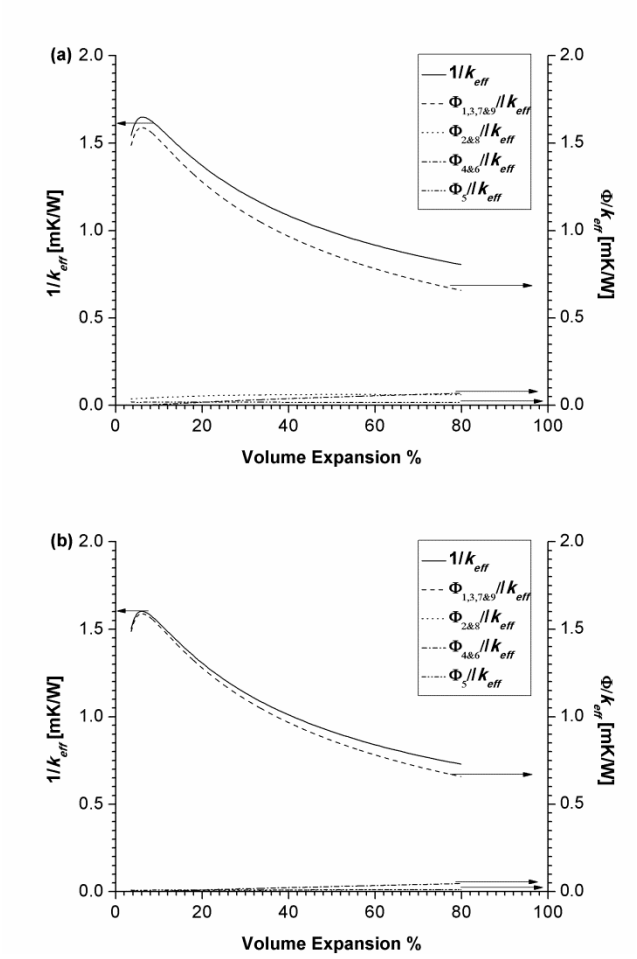

Figure 3.13 Effect of volume expansion on the $\Phi_i/k_{eff,i}$ and $1/k_{eff}$ between isotropic foaming and constrained foaming: (a) isotropic foaming; (b) constrained foaming with $a_z/a_x = 10$.

3.2.5 Effect of anisotropy of filler's thermal conductivity on PMC foam's k_{eff}

The effect of anisotropy of filler's thermal conductivity, which could be quantified as $k_{f//}/k_{f\perp}$, on PMC foam's k_{eff} was also investigated using the developed model. Figure 3.14 plots the changes of PMC foams' k_{eff} with their volume expansion percent at different values of $k_{f//}/k_{f\perp}$. The base case has $k_{f//}/k_{f\perp}$ equaled to 150 (i.e., $k_{f//}$ = 300 $W \cdot m^{-1} \cdot K^{-1}$ and $k_{f\perp}$ = 2 $W \cdot m^{-1} \cdot K^{-1}$) and the geometric mean of $k_{f//}$ and $k_{f\perp}$ were kept as constant (i.e., $(300 \times 2)^{0.5}$) in all calculations. It is observed that a higher degree of anisotropy of filler's thermal conductivity would increase

the sensitivity of the PMC foam's k_{eff} to the change in the foam's volume expansion. In other words, effectiveness of using foaming as a fabrication strategy to promote PMC's k_{eff} would increase with the anisotropy of filler's thermal conductivity.

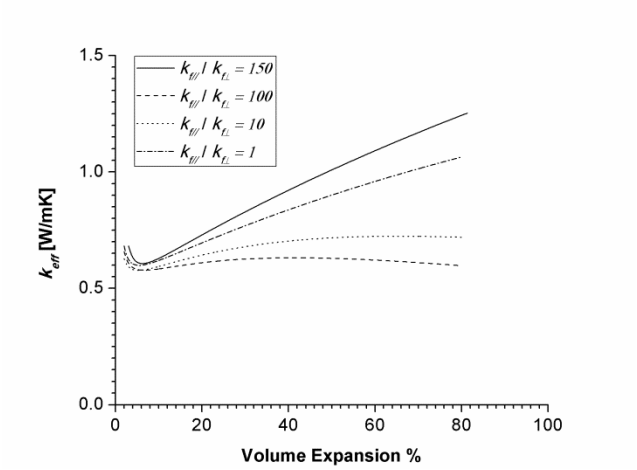

Figure 3.14 Effect of anisotropy of filler's thermal conductivity on LLDPE-hBN foam's k_{eff} (note: hBN vol.% = 10 vol.%).

3.3 Conclusion

An analytical model has been developed to predict PMC foams' k_{eff}. The PMC foam's k_{eff} predicted by this model was higher than experimental measurements of k_{eff} obtained for linear low density polyethylene LLDPE- hBN composite foams [18]. The discrepancy was believed to be caused by ignoring the thermal contact resistance between different materials as well as the over estimation of hBN's in-plane thermal conductivity. However, the trend of the calculated results demonstrated satisfactory agreement with experimental data [18]. This demonstrated that the developed model can serve as a tool to study the underlying factors that govern the PMC foam's k_{eff} and provide new insights for developing thermally conductive PMC foams. The model revealed that there is a threshold volume expansion percent over which the PMC foam's

k_{eff} would be promoted. This could be attributed not only to the enhanced filler alignment by the foaming-induced extensional stress but also to the geometric evolution of different layers (e.g., layers with only polymer, layers with polymer and filler, and layers with polymer, filler, and air void) in the PMC foams. Furthermore, parametric studies were conducted to investigate the effects of foam morphology and filler's anisotropic thermal conductivity on the PMC foam's k_{eff}. It was found that higher foam expansion percent by increasing cell population density and constrained foaming to promote expansion in the heat flow direction would enhance the PMC foam's k_{eff}. Moreover, the effectiveness of using foaming as a fabrication strategy to promote PMC's k_{eff} would increase with the anisotropy of filler's thermal conductivity. These findings provide new insights to design the morphology of PMC foams for light weight and/or flexible thermally conductive polymeric material systems with promoted k_{eff} and good processability.

Chapter 4

Parametric Study of Foam Morphology's Effects on PMC Foam's k_{eff}

The analytical study carried out in Chapter 3 demonstrates that foaming-assisted filler networking is a viable strategy to enhance the PMC's k_{eff}, especially with low filler loadings. In this context, an experimental study was conducted using low density polyethylene (LDPE)-hexagonal boron nitride (hBN) composite foams blown by Expancel® microspheres as a case example. Samples with different hBN sizes, hBN loadings and foam morphologies have been prepared to parametrically investigate the effects of filler loading, filler size, volume expansion percent, cell size and cell population density on PMC foam's k_{eff}.

4.1 Experimental

4.1.1 Materials

Commercially available LDPE (Nova Chemicals, NovaPol, LA-0219-A) was used as the matrix material in this work. Micron-scale and submicron-scale hBN platelets (PolarTherm powder grade PT110 and AC6041) were purchased from Momentive Performance Materials Inc. Expancel® microspheres (Akzonobel, 980 DU 120) were employed as the foaming agent to create cellular structures in the LDPE-hBN composites. Table 4.1 – 4.3 summarize the physical

properties of LDPE, hBN, and Expancel® microspheres, respectively [88, 91, 94]. The selection of materials was based on several rationales. Expancel® microspheres are very small spherical particles that consist of a plastic shell encapsulating a gas. Their volume increases dramatically when they are heated to their activation temperature (i.e., soften their shells and increase their internal pressure). Since the activation temperature for expanding Expancel® microspheres is 157-173 °C, LDPE, which has its melting point lower than the microsphere's onset temperature, was chosen to decouple the melting and foaming processes. hBN micron-scale and submicron-scale platelets, which possess highly anisotropic thermal conductivity, were selected to demonstrate the effect of foaming-assisted filler alignment on the PMC's keff. Moreover, their relatively low Knoop hardness (i.e., 11 kg/mm2) and graphite-like layered structure are advantageous for composite processing. The use of Expancel® microspheres as the foaming agent was due to the possibility to precisely control the PMC's foam morphology (i.e., cell population density, cell size, and volume expansion).

Table 4.1 Physical parameters of LDPE

Property	**Value**	**Unit**
Density (ρ)	918	kg/m^3
Melting temperature (T_m)	105-115	°C
Thermal conductivity (k)	0.30-0.34	$W \cdot m^{-1} \cdot K^{-1}$
Dielectric strength	27	MV/m

Table 4.2 Physical parameters of hBN

Property	Value		Unit
	PT110	**AC6041**	
Density (ρ)	2280	2280	kg/m^3
In-plane thermal conductivity ($k_{//}$)	300+	300+	$W \cdot m^{-1} \cdot K^{-1}$
Through-plane thermal conductivity ($k_{\perp}$)	~3	~3	$W \cdot m^{-1} \cdot K^{-1}$
Lateral size	45	6	µm
Thickness	1-3	0.1-0.5	µm
Specific surface area	0.6	8	m^2/g

Table 4.3 Physical parameters of Expancel 980 DU 120

Property	Value		Unit
	Pre-expansion	**Post-expansion**	
Density (ρ)	1100	30	kg/m^3
Size	25-40	120	µm
Activation Temp.	157-173	-	°C
Shape	Spherical	Spherical	-

4.1.2 Sample Preparation

Table 4.4 summarizes the material composites of the PMC and their foam samples being studied. A previous study found that the dynamic storage modulus (G') of polymer matrix

composites filled with hBN platelet increased sharply at hBN loadings closed to 10 vol%, indicating a sudden change in the material structure (i.e., formation of interconnected filler network) [95]. As a result, the lowest filler loading studied in this work was chosen to be 9.21 vol%. Although PMC can be fabricated by several processing technologies, including melt-compounding and dry-blending, previous studies revealed that dry-blended PMC samples yielded higher k_{eff} than those prepared by melt-compounding [47]. Therefore, in this study, both the solid LDPE-hBN mixtures and the foamable LDPE-hBN mixtures were prepared by dry-blending. The overall procedures to prepare PMC samples for the measurements of their k_{eff} are illustrated in Figure 4.1. Initially, LDPE pellets were ground into fine powders with particle sizes ranging from 250 μm to 500 μm by a mill freezer (SPEX SamplePrep Group, model 6770, Freezer/Mill). Calculated amounts of hBN, LDPE and Expancel® microspheres were weighed and dry-blended by continuous tumbling action at room temperature. The mixtures were then compression-molded into cylindrical samples of 20 mm in diameters and 10 mm in thicknesses by the following procedures:

1. The dry-blended powders were compacted, by a compression molding machine (Carver Press, 4386 CH), into cylindrical mold cavities at room temperature for 1 minute under a pressure of 20 MPa. The compacting step aimed to reduce the chance of undesired void formation within the compression-molded samples.

2. The compacted mixtures were heated to 125°C at 5 MPa and equilibrated at the set temperature for 25 minutes to completely melt the LDPE matrix.

3. The temperature was subsequently raised to 180°C and maintained at that temperature for 5 minutes to activate the expansion of Expancel® microspheres.

4. The compression-molded samples were transferred to a cooling module and clamped between a pair of cooling plates with flowing water channels to solidify the samples.

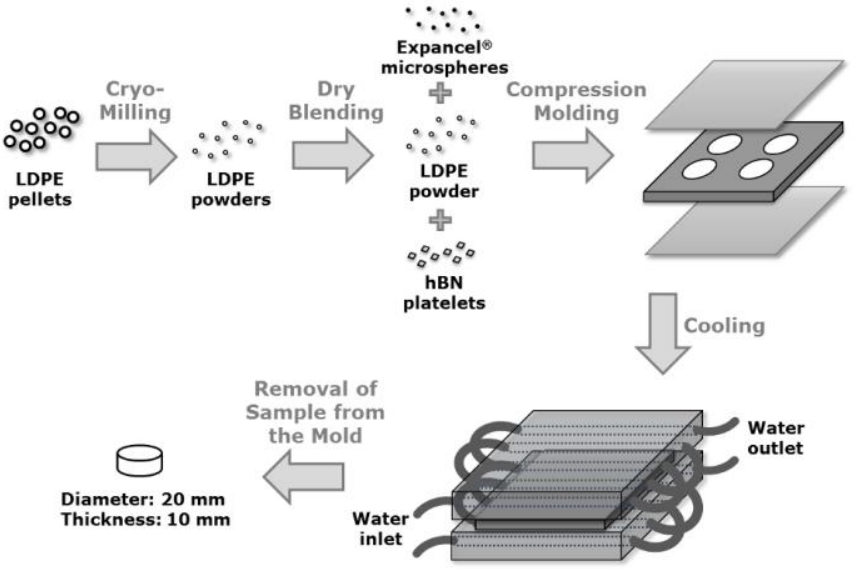

Figure 4.1 Procedures of sample preparation.

The same procedures were applied to fabricate both solid and foamed PMC samples to ensure all samples experienced the same thermal history. For solid PMC samples, the mold cavities were fully filled with the desired compositions of dry-blended LDPE-hBN mixtures without the addition of Expancel® microspheres. For PMC foam samples, the mold cavities were partially filled to a predefined volume percentage in order to control the volume expansion percent of the samples. Upon the expansion of the microspheres, the partially-filled mold cavity would be completely filled by the expanded material systems. For example, the mold cavities were 50% filled to fabricate PMC foam samples with 100% volume expansion.

The cellular morphology of the PMC foams was precisely controlled by the volume percent of the unfilled mold cavities as well as the amount of Expancel® microspheres. The volume expansion percent of the PMC foam was controlled by the percentage of mold filling. Assuming all microspheres would be expanded to their maximum sizes (i.e., 120 μm), the minimum loading of Expancel® microspheres can be estimated by Equation (4.1):

$$m = \frac{V_{void} d_o^3 \rho}{d_{\max}^3} \tag{4.1}$$

where m is the minimum required mass of Expancel® microspheres, V_{void} is the volume of the free space in mold (i.e. volume of mold minus total volume of LDPE and hBN), d_o is the diameter of unexpanded microspheres, d_{max} is the maximum diameter upon fully expansion; and ρ is the density of unexpanded Expancel® microspheres (as indicated in Table 4.3).

Table 4.4 Material compositions of PMC samples being studied

Filler Loading	Volume Expansion	Expancel® Loading
9.21 vol% hBN_{AC6041}	0%	n/a
	25%	1×, 1.5×, 2.5×, 5×, 10×
	50%	1×, 1.5×, 2.5×, 5×, 10×
	75%	1×, 1.5×, 2.5×, 5×, 10×
	100%	1×, 1.5×, 2.5×, 5×, 10×
9.21 vol% hBN_{PT110}	0%	n/a
	25%	2.5×
	50%	2.5×
	75%	2.5×
	100%	2.5×
27.63 vol% hBN_{AC6041}	0%	n/a
	25%	2.5×
	50%	2.5×
	75%	2.5×
	100%	2.5×

In order to vary the cell size and/or the cell population density of the PMC foams, the microsphere contents were varied to different multiples (*n*) of the minimum required amount calculated by Equation (4.1). In particular, *n* was varied at 1×, 1.5×, 2.5×, 5×, and 10× to generate PMC foams with different cell population densities and cell sizes. The theoretical average cell sizes for different loadings of microspheres, which are summarized in Table 4.5, can be calculated by Equation (4.2):

$$d = \frac{d_{\max}}{\sqrt[3]{n}} \tag{4.2}$$

where d is the theoretical average cell size and d_{max} is the maximum cell size when the microsphere is fully expanded.

Table 4.5 Theoretically calculated sizes of expanded Expancel® microspheres

Multiple of required microspheres loading (*n*)	Average Cell Size
1	120 µm
1.5	104 µm
2.5	88 µm
5	70 µm
10	56 µm

4.1.3 Sample Characterization

The hBN's dispersion and/or foam morphology of LDPE-hBN composites and their foams were observed by scanning electron microscopy (FEI Company, Quanta 3D FEG). Samples' cross-sections were exposed by cryo-fracturing PMC samples under liquid nitrogen. The fractured surface was sputter-coated with gold (Denton Vacuum, Desk V Sputter Coater).

The k_{eff} of LDPE-hBN composites and their foams were measured with a thermal conductivity analyzer (TCA) in accordance to ASTM E1225 [96]. The k_{eff} of three samples of each composition were measured for subsequent analyses. The average values and the standard deviations for all compositions were calculated and reported. One-way Analysis of Variance (ANOVA) was employed to test the significance of the dependence of k_{eff} on different

parameters related to the PMC foam's cellular morphology. The volume expansion percent (*VE%*) of PMC foams were determined by Equation (4.3):

$$VE\% = \left(\frac{V_{foam} - V_{solid}}{V_{solid}} \right) \times 100\% \tag{4.3}$$

where V_{foam} is the volume of the PMC foam sample and V_{solid} is the volume of the solid portion (i.e., LDPE and hBN) of the sample.

In order to investigate the effects of hBN and foam expansion on the crystalline structure of the LDPE and LDPE composites, X-ray diffraction analyses were conducted using a Philips Analytical X-ray diffractometer equipped with a Cu anode running at 40 kV and 40 mA. The scanning was carried out in an angular region (2θ) ranging from 10° to 60°, with a step size of 0.02 °/min and time-per-step of 2 s. The obtained X-ray diffraction spectra were analyzed with X-Pert system software. The crystalline sizes were determined by the Scherrer equation [97], shown in Equation (4.4):

$$L = \frac{K\lambda}{\beta \cos\theta} \tag{4}$$

where K is the Scherrer constant, λ is the wavelength of the X-ray, β is the breadth of the diffraction peak, and θ is half of the diffraction angle.

4.2 Results and Discussion

4.2.1 Effects of hBN Platelet Sizes and Contents on PMC's k_{eff}

Figure 4.2 plots the effects of hBN contents on the k_{eff} of solid LDPE-hBN composites filled with either micron-scale hBN platelets (i.e., hBN_{PT110}) or submicron-scale hBN platelets (i.e., hBN_{AC6041}). Regardless of the platelet's size, the PMC's k_{eff} increased with hBN loadings, ranging from 0 vol% to 30 vol%. While the size of hBN platelets showed negligible effect on the PMC's k_{eff} at low hBN loading (e.g., 9.21 vol%), PMC filled with submicron-scale hBN platelets demonstrated more pronounced enhancement on the PMC's k_{eff} at higher hBN loadings (e.g., 18.42 vol% and 27.63 vol%). At low hBN loading, the population density of hBN platelets was not sufficient to establish a thermally conductive network in the LDPE matrix. Therefore, PMC's k_{eff} solely depended on the hBN content at low hBN loading (i.e., 9.21 vol% or less). However, hBN platelets were able to form an interconnected network in the LDPE matrix at a high hBN loading. Considering that the specific surface areas for hBN_{PT110} and hBN_{AC6041} are 0.6 m^2/g and 8.0 m^2/g, respectively, the submicron hBN platelet (i.e., hBN_{AC6041}) would have a higher efficiency to form a thermally conductive network. Therefore, the corresponding LDPE-hBN composite's k_{eff} increased more rapidly with higher hBN loadings. Nevertheless, no percolation-like behavior was observed in the relationship between hBN loading and PMC's k_{eff}. This could be attributed to the phonon scattering at the filler-filler interfaces, which is detrimental to heat conduction, despite the establishment of filler network [23, 27]. Although the measured k_{eff} of solid PMCs didn't show obvious evidence in the formation of thermally conductive hBN network in LDPE-hBN composites with 9.21 vol% of hBN loading, a sudden change in the

material structure (i.e., formation of interconnected filler network) at hBN loading close to 10 vol% was suggested by a previous research [95]. Furthermore, the LDPE-hBN composite filled with 27.63 vol% of hBN demonstrated clear evidence of filler interconnection with the measured k_{eff} values. In order to explore how foam expansion could promote the formation of filler network, foamed PMCs with both 9.21 vol% and 27.63 vol% of hBN loading were studied in greater details and presented in following sections. Moreover, the measured k_{eff} of solid PMCs would also be used as a base case to evaluate the feasibility and effectiveness of foaming-assisted filler alignment to promote PMC's k_{eff}, especially for PMC with low filler loadings.

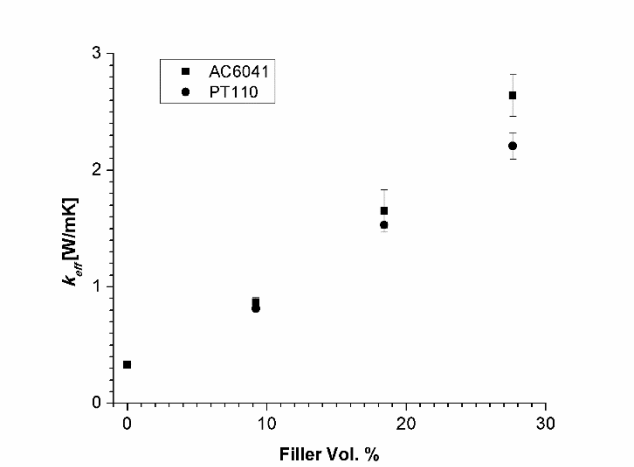

Figure 4.2 Effects of hBN platelet sizes and contents on the LDPE-hBN composite's k_{eff}

4.2.2 Effects of Volume Expansion of PMC Foams on Their k_{eff}

Thermally conductive thermoplastic-ceramic composite foams with lower mass density and similar k_{eff} comparing to their solid counterparts had recently been reported [18]. However, as far as the literature survey goes, PMC foams with their k_{eff} higher than solid PMC with the same filler loading have never been achieved. In this context, a series of parametric studies

were conducted to systematically elucidate the underlying mechanisms for the cellular morphology of a PMC foam influences the foam's k_{eff}.

LDPE-hBN composites filled with different hBN loadings and hBN platelets of different sizes were foamed to investigate the effect of volume expansion percent on PMC foam's k_{eff}. Figure 4.3 shows the representative SEM micrographs of these LDPE-hBN foams. Figure 4.3(a) and 4.3(b) illustrate that the micro-scale hBN_{PT110} platelets and submicron-scale hBN_{AC6041} platelets were preferentially aligned around expanded microspheres in LDPE-hBN foams. Both samples were foamed by 2.5× Expancel® microspheres to volume expansions of 25%. While hBN platelets were randomly oriented in the LDPE matrix, the expansion of microspheres generated biaxial stretching along their cell walls, and thereby induced the preferential alignment of the platelets along the cell walls around expanded microspheres. It can be observed that the submicron-scale platelets were able to form a more interconnected thermally conductive network than the micron-scale platelets. This can be attributed to the significantly larger (i.e., slightly over 13-fold) specific surface area of the submicron-scale platelets than that of the micron-scale platelets. Figures 4.3(c) and 4.3(d) depict that, for PMC foams filled with either hBN_{PT110} or hBN_{AC6041}, increasing the volume expansion percent from 25% to 75% would potentially block the formation of thermally conductive pathway because of the close proximity of adjacent expanded microspheres.

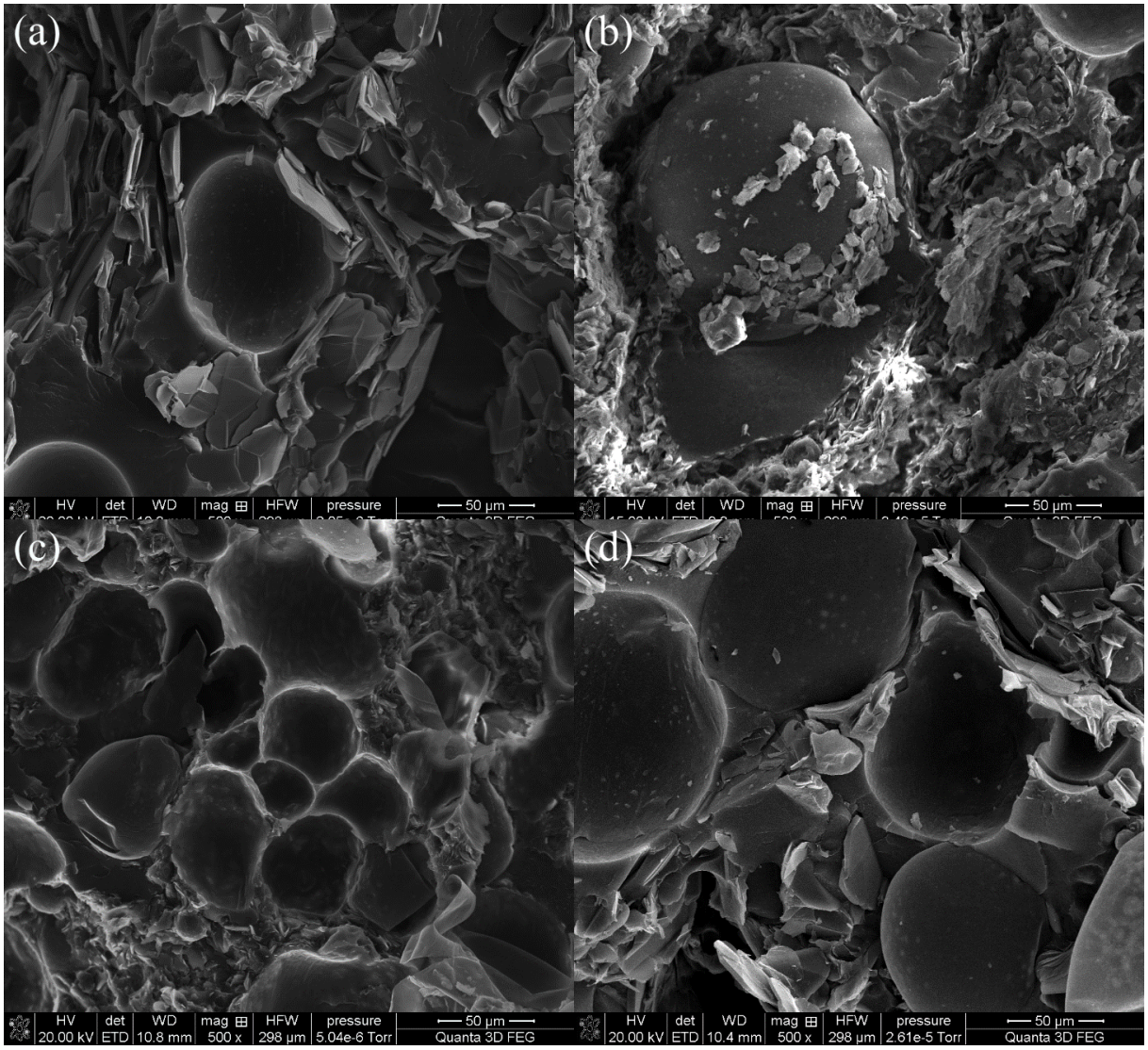

Figure 4.3 SEM micrographs of LDPE-hBN composite foams filled with 9.21 vol% hBN and 2.5× of Expancel® microspheres: (a) hBN_{PT110} & 25% volume expansion; (b) hBN_{AC6041} & 25% volume expansion; (c) hBN_{AC6041} & 75% volume expansion; and (d) hBN_{PT110} & 75% volume expansion

Figure 4.4 plots the effect of volume expansion percent on k_{eff} of LDPE-hBN foams filled with different types or loadings of hBN platelets. At 9.21 vol% filler loading, moderate foam expansion (e.g., 25%) of LDPE-hBN foams filled with either hBN_{PT110} or hBN_{AC6041} platelets enhanced the PMC's k_{eff}. In contrast, volume expansions beyond 50% were detrimental to the PMC foam's k_{eff}. For PMC foams with 25% volume expansion, the k_{eff} of LDPE-hBN foam filled

with hBN_{AC6041} platelets was 1.16 $W \cdot m^{-1} \cdot K^{-1}$, which represented a 26% increase over that of its solid counterparts. The improved k_{eff} for LDPE-hBN foam filled with 9.21 vol% of hBN_{PT110} platelets and a volume expansion percent of 25% was 0.97 $W \cdot m^{-1} \cdot K^{-1}$, which was equivalent to a 21% increase over that of the solid composite. These results represent the first time PMC foams with their k_{eff} higher than solid PMC embedded with the same filler loadings were fabricated. The more pronounced positive effect of moderate foam expansion on k_{eff} of PMC filled with hBN_{AC6041} could be caused by the higher efficiency of submicron-scale hBN platelets to establish interconnecting filler network in the LDPE matrix. One-way ANOVA tests were conducted to verify the dependence of PMC foams' k_{eff} on the foams' volume expansion percent. Table 4.6 summarized the statistical results of the one-way ANOVA tests. The results indicate that the effect of PMC foam's volume expansion percent on the foam's k_{eff} was significant for PMC foams filled with 9.21 vol%, hBN_{AC6041}, 9.21 vol% hBN_{PT110} and 27.63 vol% hBN_{AC6041}. The mound-shape k_{eff}-to-volume expansion relationship reveals that there would be two or more competing factors that governed PMC foam's k_{eff}. Unlike LDPE-hBN foams filled with 9.21 vol% hBN platelets, the k_{eff} of PMC foams loaded with 27.63 vol% hBN_{AC6041} platelets decreased monotonically as their volume expansion percent increased.

Table 4.6 One-way ANOVA tests for the dependence of PMC foams' k_{eff} on PMC foam's volume expansion %

Testing Parameter	Data Set	*P*-Value	Significance
Volume Expansion %	9.21 vol% hBN_{AC6041}	7.2×10^{-7}	>99%
	9.21 vol% hBN_{PT110}	8.8×10^{-5}	>99%
	27.63 vol% hBN_{AC6041}	1.1×10^{-6}	>99%

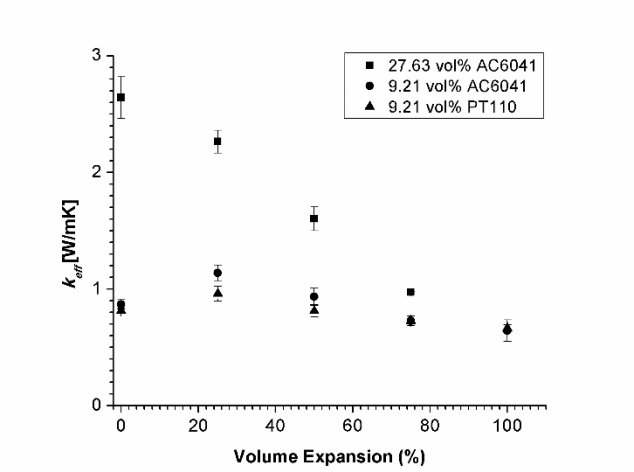

Figure 4.4 Effect of volume expansion % on k_{eff} of LDPE-hBN composite foamed by 2.5× Expancel® microspheres

For LDPE-hBN foams filled with 9.21 vol% hBN platelets, the positive effects of foaming on PMC's k_{eff} include (i) foaming-assisted filler alignment along the cell walls (i.e., Figure 3 (a) and (b)); and (ii) localization of hBN platelets in the solid phase of the PMC foam. The effective filler content in the PMC foam's solid region can be determined by Equation (4.5):

$$effective\ filler\ content = \frac{\phi_{filler}\left(V_{solid} + V_{void}\right)}{V_{solid}} \times 100\% \quad (4.5)$$

where ϕ_{filler} is the volume fraction of hBN platelets in the PMC, V_{solid} is the volume of the solid phase in the PMC foam, and V_{void} is the total volume of all voids in the PMC foam.

The presence of foaming-induced filler alignment was evident in Figure 3(a) and 3(b). The preferential orientation of hBN platelets along the cell wall of expanded microspheres would promote the interconnectivity of the hBN platelets, leading to a positive impact on the PMC foam's k_{eff}. Figure 4.5 shows how PMC foam's volume expansion would increase the effective filler content in the solid phase. For example, a 25% volume expansion of LDPE-hBN foams filled with 9.21 vol% hBN platelets would result in an effective hBN content of 11.51 vol%. Such hBN platelets localization in the LDPE matrix would result in a higher probability of filler networking, and thereby promoting the PMC foam's k_{eff}.

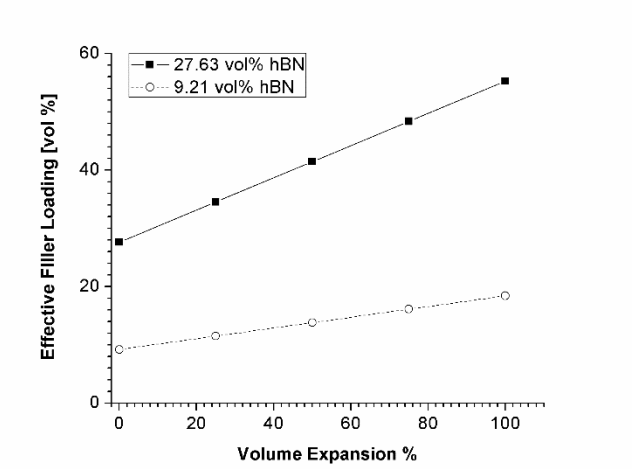

Figure 4.5 Effective filler loading with respect to different volume expansion %

In contrast, the negative influence of foaming on LDPE-hBN composite foam's k_{eff} could be attributed to (i) the introduction of thermally insulating voids in the polymer matrix; and (ii) the disruption of hBN filler network between adjacent cells. It is obvious that increasing PMC foam's volume expansion percent would raise the volume fraction of thermally insulating voids, and be detrimental to the PMC's k_{eff}. Moreover, as indicated in Figure 4.3(c), close proximity of expanded microspheres in excessively expanded PMC foams would disrupt the establishment of hBN filler network. This would also have a negative impact on the PMC's k_{eff}. At 27.63 vol% hBN loading, the omnipresence of hBN platelets had guaranteed an excessive interconnected hBN network in the LDPE matrix. Therefore, further increase in effective filler concentration in localized region would have minimal impact on further promoting filler interconnectivity, and thereby overall thermally conductive network. This explains why the PMC's k_{eff} decreased monotonically as the volume expansion percent and the fraction of thermally insulating voids increased.

4.2.3 Effects of Cell Size of PMC Foams on Their k_{eff}

Using the methods described in the experimental section, PMC foams were fabricated to study the effect of cell size on the k_{eff} of PMC foams at four levels of volume expansion percent (i.e., 25%, 50%, 75% and 100%). Figure 6 plotted the measured k_{eff} of LDPE-hBN_{AC6041} with 9.21 vol% of hBN platelets and controlled foam expansion percent against cell size. For the LDPE-hBN_{AC6041} foams with 25% and 50% volume expansion, it was observed that the PMC foam's k_{eff} can be promoted by moderate cell size growth; whereas excessive cell expansion would lead to a reduced k_{eff}. In contrast, the k_{eff} of PMC foams with volume expansion of 75%

and 100% seems to be insensitive to the change in cell size. One-way ANOVA tests have been performed, and the results are summarized in Table 4.7. It is verified that the effect of filler size on PMC foam's k_{eff} is significant for PMC foams with volume expansion of 25% and 50%.

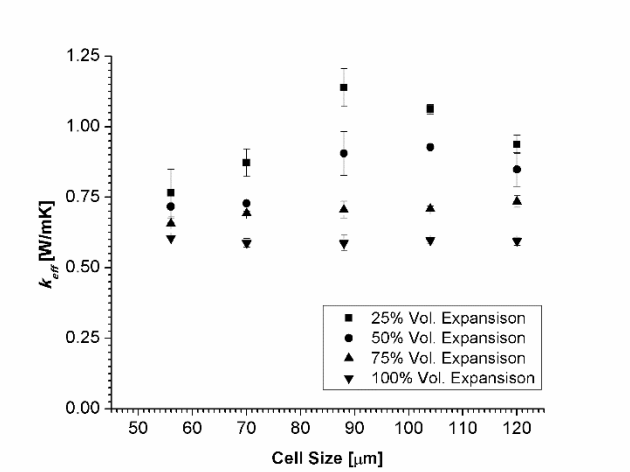

Figure 4.6 Effect of cell size on the k_{eff} of LDPE-hBN_{AC6041} foams filled with 9.21 vol% hBN and with different volume expansion %

Table 4.7 One-way ANOVA tests for the dependence of PMC foams' k_{eff} on PMC foam's cell size

Testing Parameter	**Data Set**	***P*-Value**	**Significance**
Cell Size	25% volume expansion	7.9×10^{-4}	>99%
	50% volume expansion	3.0×10^{-3}	>99%
	75% volume expansion	0.043	>95%
	100% volume expansion	0.828	<18%

The mound-shape k_{eff}-to-cell size relationship that possessed by PMC foams with 25% and 50% volume expansion suggested that cell growth would bring both positive and negative effects on the PMC foam's k_{eff}. At each constant volume expansion percent, the effect of filler localization induced by foam expansion in the solid phase would be comparable. Therefore, the positive effect was solely attributed to the different levels of cell expansion-induced biaxial stress field, which helps hBN platelets align around the cell wall. Such preferential alignment and enhanced networking of submicron-scale hBN platelets by foaming in a LDPE matrix is illustrated in Figure 7. This observation was consistent with other studies on foaming-induced enhancement in PMC's mechanical or electrical properties [62, 90]. The foaming-induced biaxial stress field increased with bubble expansion, and thereby resulting in higher degree of filler alignment along the cell wall to establish a thermally conductive network. However, once the cell expansion reached the critical level (i.e., most hBN platelets become preferentially aligned tangentially around the expanded microspheres, further biaxial stretch would potentially result in the breaking of thermally conductive network, and suppressing the PMC foam's k_{eff} as illustrated with the schematics in Figure 4.8. This phenomenon is consistent with similar observations in electrically conductive polymer-carbon nanotubes nanocomposites [90].

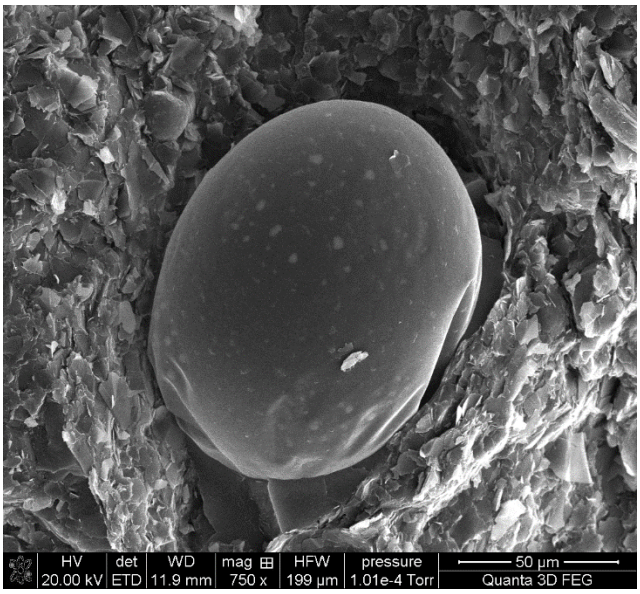

Figure 4.7 Foaming-assisted alignment of hBN_{AC6041} platelets around an expanded bubble in a 25% expanded PMC foam (with 9.21 vol% hBN_{AC6041} & 2.5× Expancel® microspheres)

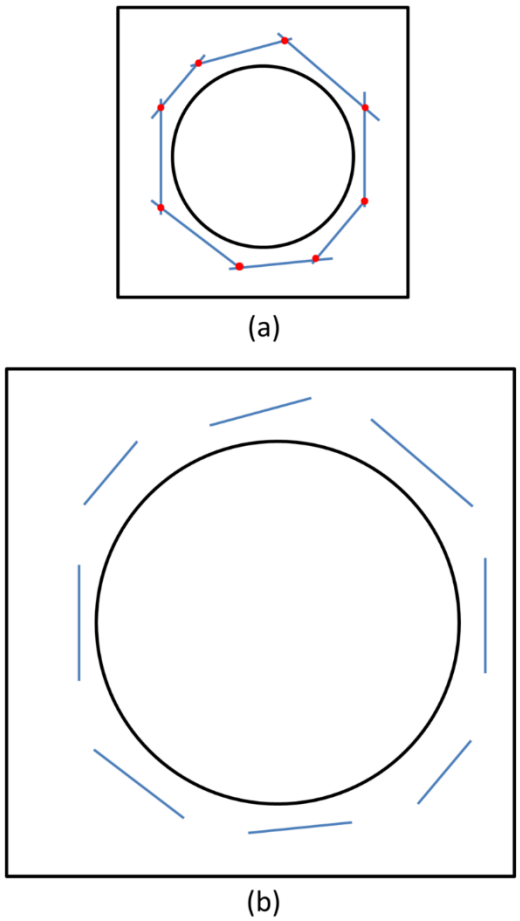

Figure 4.8 Schematics of cell expansion-induced filler connection disruption: (a) enhanced filler connection by foaming-induced filler alignment; and (b) filler disconnection induced by excessive cell expansion

Secondly, the difference in the sensitivity of PMC foam's k_{eff} on cell size indicated that cell expansion-induced effects are more significant in PMC foams with low volume expansion percent. When the PMC foam has high volume expansion percent, the high volume fraction of thermally insulating air voids became the predominant factor on the PMC foam's k_{eff}. This phenomenon could be attributed to the blockage of filler network, as illustrated in Figure 4.3(c). Considering the air voids have a simple cubic arrangement, Equation (4.6) was used to

determine the average cell-to-cell distance. The calculated cell-to-cell distance under different volume expansion percent and cell sizes are summarized in Table 4.8.

$$D = (\sqrt[3]{(\frac{VE\% + 1}{VE\%})\frac{\pi}{6}} - 1) \cdot d \quad (4.6)$$

where *D* is the average cell-to-cell distance, *VE%* is the volume expansion % and *d* is the average cell size

Table 4.8 Theoretically calculated average cell-to-cell distance under different combination of Expancel® loading and volume expansion percent disappoint

Average Cell Size [µm]	Average cell-to-cell distance [µm] (D)			
	25% Volume Expansion	50% Volume Expansion	75% Volume Expansion	100% Volume Expansion
120	45.4	19.4	8.2	1.86
104	39.6	17.0	7.2	1.62
88	33.4	14.4	6.2	1.36
70	26.6	11.4	4.8	1.08
56	21.0	9.0	3.8	0.86

For PMC foams with low volume expansion (i.e. 25% and 50%), the estimated cell-to-cell distances were relatively large. For these foams, the aforementioned positive and negative effects of cell size contributed to the mound-shaped curve. However, as the PMC foam's volume expansion increased, adjacent cells became closer to each other. For example, the estimated cell-to-cell distances were less than 2 µm for PMC foams with 100% volume expansion. Therefore, with the random dispersion of the microspheres in the LDPE matrix, it was highly probable that cells would be in contact with each other and completely avoid the

formation of a thermally conductive path in some regions (as shown in Figure 4.3(c)). This significantly suppressed the PMC foam's k_{eff}, and the influence of cell size on PMC foams' k_{eff} became negligible.

4.2.4 Effects of Cell Population Density of PMCs on Their k_{eff}

In order to study the effect of cell population density on the PMC foam's k_{eff}, PMC foams were fabricated with two different cell population densities by changing the amount of Expancel® microspheres (i.e., 0.029 g/cm^3 and 0.058 g/cm^3 with respect to the solid volume) being embedded in the LDPE matrices. All samples were filled with 9.21 vol% of hBN_{AC6041} and with different volume expansion percent (i.e. 25%, 50%, 75% and 100%).Figure 4.9 plotted the k_{eff} of PMC foams at two different levels of cell population density (i.e., 1.4×10^6 cells/cm^3 and 2.8×10^6 cells/cm^3 with respect to unfoamed volume) against different levels of volume expansions. Experimental results revealed that the dependences of PMC foam's k_{eff} on the volume expansion percent were different for foams with different cell population densities. It was found that the PMC foams with lower cell population density (i.e., 1.4×10^6 cells/cm^3 with respect to unfoamed volume) had a mound-shaped k_{eff}-to-volume expansion relationship and the maximum k_{eff} occurred at approximately 50% volume expansion. In contrast, the k_{eff} of PMC foams with cell density of 2.8×10^6 cells/cm^3 with respect to unfoamed volume showed a monotonically decreasing trend. Overall, it can be observed that the k_{eff} of PMC foams with volume expansion of 75% and 100% seems to be insensitive to the change in cell population. One-way ANOVA tests have been performed, and the results are summarized in Table 4.9. It is

verified that the effect of cell population density on PMC foam's k_{eff} is significant for PMC foams with volume expansion of 25% and 50%.

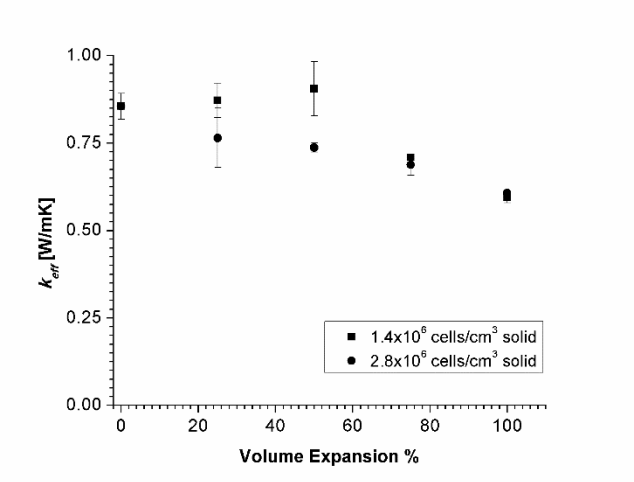

Figure 4.9 Effect of cell population density on the LDPE-hBN$_{AC6041}$ composite's k_{eff}

In order to understand the different behaviors caused by these two levels of cell densities, it must be noted that the three morphological parameters, cell size, volume expansion percent, and cell population density are interrelated. In other words, each of the three parameters is determined simultaneously by the other two. Moreover, the average cell size will be larger to increase volume expansion percent without changing the cell population density, the average cell size also needs to be increased. At a fixed cell population density, the average cell size can be calculated as a function of volume expansion percent using Equation (4.7). Figure 10 plotted the calculated average cell size as a function of the foam's volume expansion percent at the aforementioned two levels of cell population densities.

$$d = \sqrt[3]{\frac{6 \times VE\%}{\pi N}} \tag{4.7}$$

where *d* is the average cell size, *VE%* is the volume expansion % and *N* is the number of cells per unit volume of solid.

Table 4.9 One-way ANOVA test for the dependence of PMC foams' k_{eff} on PMC foam's cell population density

Testing Parameter	Data Set	*P*-Value	Significance
Cell Population Density	25% volume expansion	0.130	87%
	50% volume expansion	0.094	>90%
	75% volume expansion	0.906	<10%
	100% volume expansion	0.553	<50%

For the PMC foams with a cell population density of 1.4×10^6 cells / cm^3 with respect to unfoamed volume, the cell size increased from approximately 70 µm to 111 µm as the volume expansion percent varied from 25% to 100%. The maximum k_{eff} occurred at 50% volume expansion. Figure 4.10 showed that the corresponding cell size is around 88 µm, which was consistent with the result in Figure 4.6. In other words, the initial increasing trend could be attributed to the cell expansion-induced filler alignment, as discussed in Section 3.3. As the volume expansion percent continued to increase, the corresponding average cell size became larger. As discussed in Section 3.2 and 3.3, both excess foam expansion and cell size could disrupt the filler interconnectivity. Together with the large volume fraction of thermally insulating air, the PMC foam's k_{eff} dropped after reaching its peak at 50% volume expansion.

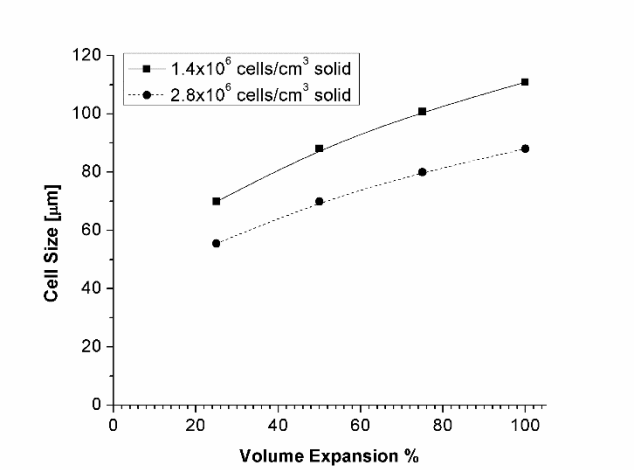

Figure 4.10 Effect of foam volume expansion on the average cell size with constant cell population density

For the PMC foams with a cell density of 2.8×10^6 cells/cm^3 with respect to unfoamed volume, as the volume expansion increased from 25% to 100%, the corresponding cell size increased from approximately 55 µm to 88 µm. In this case, the average cell sizes were smaller than that of the PMC foams with a cell density of 1.4×10^6 cells/cm^3 with respect to unfoamed volume under same volume expansion percent. For instance, the average cell size was only 55 µm for PMC foams with 25% volume expansion. The low degree of cell expansion was not sufficient to effectively align the hBN platelets along the cell wall. When the optimal cell size of about 88 µm had been reached, the corresponding volume expansion was 100%. The high volume fraction of thermally insulating air and the challenge to form an interconnected conductive filler path due to the small cell-to-cell distance would suppress the k_{eff}.

4.2.5 Effects of hBN and Foam Expansion on the Crystalline Structures of the LDPE and LDPE Composites

As shown in Figure 4.11, typical crystalline peaks of LDPE at 21.5°, 24.3° and 36.5° were observed from the X-ray diffraction (XRD) spectra of LDPE and LDPE composites, which corresponded to the orthorhombic crystallite plane 110, 200, 210, respectively [98]. The XRD spectra reveal that the addition of Expancel® and/or hBN increased both the area and full width at half maximum (FWHM) of the (110) peak, which correspond to an increase in the degree of crystalline phase and a decrease in the crystal size. Table 4.10 shows that the area of the (110) peak increased most significantly in LDPE-hBN composite foams, followed by solid LDPE-hBN composites, and then LDPE foam. This is attributed to the synergistic effect of two mechanisms, (i) stress-induced crystallization caused by the extensional stress generated around expanding bubbles [99], and (ii) enhanced crystallization by the presence of hBN platelets as the nucleating agent [100]. Furthermore, the effect of filler-induced crystallization was observed to be more prominent when smaller hBN platelets (i.e., AC6041) were used.

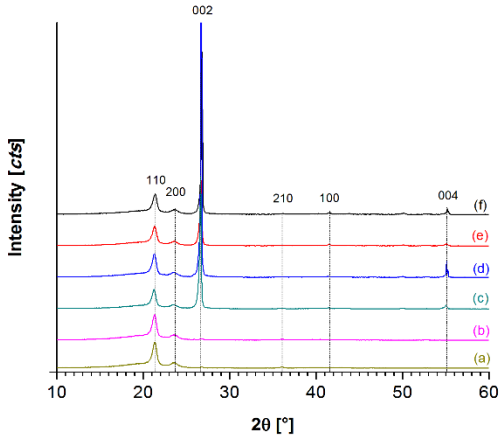

Figure 4.11 XRD spectra of the LDPE, LDPE-hBN composites, and their foams: (a) neat LDPE; (b) LDPE foam with 25% volume expansion; (c) LDPE-hBN_{AC6041} solid composite with 9.21 vol.% hBN; (d) LDPE-hBN_{PT110} solid composite with 9.21 vol.% hBN; (e) LDPE-hBN_{AC6041} composite foam with 9.21 vol.% hBN and 25% volume expansion; and (f) LDPE-hBN_{PT110} composite foam with 9.21 vol.% hBN and 25% volume expansion

Table 4.10 Effects of hBN and foam expansion on the XRD spectra of LDPE, LDPE-hBN composites, and their foams (25% volume expansion)

Composition	Peak	FWHM (°)	Peak Area (°·cts)	Crystallite Size (Å)
Neat LDPE	(110)	0.1181	367.87	676.87
LDPE Foam	(110)	0.1378	394.29	580.11
LDPE-hBN_{AC6041} Composite	(110)	0.3936	862.26	203.07
LDPE-hBN_{PT110} Composite	(110)	0.1968	529.72	406.15
LDPE-hBN_{AC6041} Composite Foam	(110)	0.4330	1062.8	184.62
LDPE-hBN_{PT110} Composite Foam	(110)	0.3936	928.13	203.11

The typical (002), (004) and (100) peaks in an XRD spectrum of hBN were found in LDPE-hBN composites in Figure 11 [101]. The (002) and (004) peaks refer to horizontally oriented hBN (i.e., the through-plane of hBN is perpendicular to the horizontal direction) while the (100) peak is related to vertically oriented hBN [102]. Table 4.11 shows the effects of hBN platelet size and foam expansion on the XRD spectra of LDPE composites. As expected, larger hBN platelets (i.e., PT110) resulted in stronger intensities and larger crystalline sizes for the (002) and (004) peaks due to the significant difference in the lateral sizes of the two hBN grades. Comparing with the solid LDPE-hBN composites, the dramatically change of the intensities of (002), (004) and (100) peaks of LDPE-hBN composite foams provide evidence of the foaming-induced change in hBN orientation in the composites.

Table 4.11 Effects of filler size and foam expansion on the XRD spectra of LDPE, LDPE-hBN composites, and their foams (25% volume expansion)

Composition	Peak	FWHM (°)	Peak Area (°·cts)	Crystallite Size (Å)
LDPE-hBN_{AC6041} Composite	(002)	0.1378	18645.68	585.85
LDPE-hBN_{PT110} Composite	(002)	0.0787	67028.77	1025.92
LDPE-hBN_{AC6041} Composite Foam	(002)	0.1771	9296.68	455.90
LDPE-hBN_{PT110} Composite Foam	(002)	0.1378	24326.56	586.03
LDPE-hBN_{AC6041} Composite	(004)	0.1680	503.64	527.21
LDPE-hBN_{PT110} Composite	(004)	0.0590	2291.83	1501.62
LDPE-hBN_{AC6041} Composite Foam	(004)	0.4320	282.96	205.07
LDPE-hBN_{PT110} Composite Foam	(004)	0.0720	841.11	1231.01
LDPE-hBN_{AC6041} Composite	(100)	0.1968	125.85	426.80
LDPE-hBN_{PT110} Composite	(100)	0.1968	94.31	426.78
LDPE-hBN_{AC6041} Composite Foam	(100)	0.2362	192.2	355.68
LDPE-hBN_{PT110} Composite Foam	(100)	0.1968	205.15	426.94

4.3 Conclusion

This study successfully fabricated thermally conductive low density polyethylene (LDPE)-hexagonal boron nitride (hBN) composite foams with their effective thermal conductivity (k_{eff}) higher than their solid counterparts. In order to explore how foaming induced filler alignment can promote the formation of such filler network, PMC foams with two levels of filler loading (i.e., 9.21 and 27.63 vol%) were studied. In particular, the k_{eff} of PMC foams filled with 9.21 vol% of hBN_{AC6041} (i.e., submicron-scale) or hBN_{PT110} (i.e., micron-scale) reached as high as 1.16 $W \cdot m^{-1} \cdot K^{-1}$ and 0.97 $W \cdot m^{-1} \cdot K^{-1}$, respectively. These values represented 26% and 21% increases over those of their solid counterparts. Parametric studies were conducted to study the effects of foam morphologies on the PMC foam's k_{eff}.

It was found that both foam volume expansion and cell size had competing effects on the PMC foam's k_{eff}. PMC foams with moderate volume expansion percent would promote the foams' k_{eff}. This was caused by the localization of fillers in the solid phase, which promoted the hBN platelets' interconnectivity. In contrast, high volume expansion percent would result in high volume fraction of thermally insulating air voids. The reduced average cell-to-cell distance would also disrupt the development of continuous thermally conductive path. Therefore, the PMC foam's k_{eff} would decrease. Similarly, large cell sizes also had both beneficial and detrimental effects on the k_{eff}. On the one hand, cell expansion would create a biaxial stress field that promoted filler alignment along the cell walls, and promoted the PMC foam's k_{eff}. On the other hand, excessive cell expansion could disrupt the development of interconnected filler network, and subsequently suppress the PMC foam's k_{eff}. Furthermore, the enhancement of

LDPE crystallization by the synergistic effect of the presence of hBN platelets and the foaming-induced crystal nucleation was shown in X-ray diffraction (XRD) analyses. The XRD spectra also reveal foam expansion led to changes in the orientation of hBN platelets.

In short, the findings of this research provided guidelines for the design and fabrication of lightweight thermally conductive PMC foams. Such thermally-conductive PMC foams would provide a new material family to assist the industry to deal with the challenge in heat management problem in their next generation products.

Chapter 5

Fabrication of Thermally Conductive PMC Foams by Physical Foaming

The focus of this thesis is to develop thermally conductive PMC foams with low filler loading. Results from Chapter 4 have demonstrated foaming as a strategy to promote PMC foam's k_{eff}. This chapter studies the fabrication of PMC composite foams using CO_2 as physical foaming agent. CO_2 is a commonly used blowing agent in the industry, and this study can test the feasibility of large scale production of thermally conductive PMC foams.

5.1 Experimental

5.1.1 Materials

In this study, the matrix material used was polylactic acid (PLA) (NatureWorks, Ingeo 8052D). The physical properties of PLA are summarized in Table 5.1 [102]. PLA is a bioplastics derived from renewable resources. Besides its sustainability, PLA also has good optical property and can be processed with standard methods (e.g., extrusion, injection molding, film and sheet casting). hBN platelets with submicron thickness (Momentive Performance Materials Inc., PolarTherm, AC6041) were used as thermally conductive filler, and the physical properties are shown in Table 4.2. hBN_{AC6041} was chosen over hBN_{PT110}, because the study in Chapter 4 showed

that it exhibited more pronounced enhancement on the PMC's k_{eff} than hBN_{PT110} at same filler loading and foam structure. Pressurized CO_2 (99.8% pure from Linde Gas Inc.) was employed as the physical foaming agent. CO_2 was chosen as the physical foaming agent, because of its relatively high solubility in plastics, low toxicity, non-flammability, good thermal and chemical stability, as well as low cost. More importantly, it is not an ozone depleting agent.

Table 5.1 Physical parameters of PLA

Property	Value	Unit
Density (ρ)	1240	kg/m^3
Melting temperature (T_m)	145-160	°C
Thermal conductivity (k)	0.11-0.19	$W \cdot m^{-1} \cdot K^{-1}$

5.1.2 Preparation of Foamable Film

In order to reduce the gas saturation time for the batch foaming process, it is important to prepare the foamable samples with small thickness. Foamable pure PLA and PLA-hBN_{AC6041} films were prepared with compression molding using the following steps:

1. Pure PLA powders or dry-blended PLA-hBN_{AC6041} mixture with pre-calculated composition were placed into a thin film mold with thickness of 500 μm, and placed into a compression molding machine (Carver Press, 4386 CH). No pressure was applied at this step.

2. The temperature was increased to 185 °C and equilibrated at the set temperature for 25 minutes to completely melt the PLA matrix.

3. A pressure of 5 MPa was applied and maintained for 5 minutes to compress the molten sample into the shape of the mold.

4. The compression-molded samples were transferred to a cooling module and clamped between a pair of cooling plates with flowing water channels to solidify the samples.

5.1.3 Procedure of Sorption Study

Before foaming, a PLA–CO_2 sorption study was conducted at room temperature with the gas pressures at 1000 psi. The saturation pressure was chosen based on results in existing literatures of CO_2 blown PLA foams [103, 104]. The sorption experiments were carried out to study the rate of uptake and the equilibrium concentration of CO_2 gas in PLA, which will help to identify the appropriate gas saturation time for the batch foaming process.

Samples measuring approximately 2.5 cm by 2.5 cm were cut from foamable films prepared with steps listed in section 5.1.2. After measuring the weight, a piece of sample was placed into a foaming chamber and saturated at 1000 psi. After a pre-determined saturation time, the sample was removed from the pressure chamber for weighing. The change in the sample's weight is equal to the weight of CO_2 absorbed by the foamable film. The CO_2 uptake can be approximated by dividing the weight difference by the original weight. Three samples were weighted for each saturation time. The saturation time was increased until the CO_2 uptake stopped changing, indicating that CO_2 concentration has reached its solubility in PLA.

5.1.4 Procedure of Foaming Study

The foamable films prepared with steps listed in section 5.1.2 were cut into square samples (approximately 2 cm by 2 cm) for the foaming process. Foam structures were obtained using a typical batch foaming process, which includes the following steps:

1. Saturate the foamable film with pressurized CO_2 (1000psi) in a foaming chamber at room temperature for 1 hour.

2. Rapidly depressurize the foaming chamber and remove the saturated sample.

3. Load the saturated sample into a foaming mold and submerge the mold into oil a bath with controlled temperature (i.e. 100 °C, 110 °C, 120 °C, 130°C or 140 °C).

4. Put the sample, along with the foaming mold, into ice-water to stabilize the foam structure.

5.1.5 Sample Characterization

The apparent density of foamed samples is obtained by measuring its weights in air and in water. The process and setup was in accordance to ASTM D1622 [105]. Equation 5.1 was used to calculate the apparent density from the weights measured in air and water.

$$\rho = \frac{m_{air}\rho_{water}}{m_{air} - m_{water}} \tag{5.1}$$

where ρ is the apparent density of sample, m_{air} is the sample's weight measured in air, m_{water} is the sample's weight measured in water, and ρ_{water} is the density of water.

The hBN's dispersion and/or foam morphology of PLA foams and PLA-hBN composite foams were observed by scanning electron microscopy (FEI Company, Quanta 3D FEG). Samples' cross-sections were exposed by cryo-fracturing PMC samples under liquid nitrogen. The fractured surface was sputter-coated with gold (Denton Vacuum, Desk V Sputter Coater). Finally, the k_{eff} of PLA-hBN composites and their foams were measured with a thermal conductivity analyzer (TCA) in accordance to ASTM D5470 [106].

5.2 Results and Discussion

5.2.1 Sorption Study

The CO_2 saturation results of neat PLA samples are shown in Figure 5.1. The equilibrium CO_2 concentration in PLA at 1000 psi and room temperature was found to be approximately 230 µg CO_2 per g of PLA (23 wt.%). Such concentration is comparable to previous CO_2 sorption study in PLA, which reported 21 wt.% CO_2 uptake at 5 MPa (approximately 725 psi) [103]. The results also suggested that the samples can reach equilibrium in less than 1 hour of saturation. As a results, all neat PLA samples were saturated under 1000 psi for 1 hour in subsequent foaming studies.

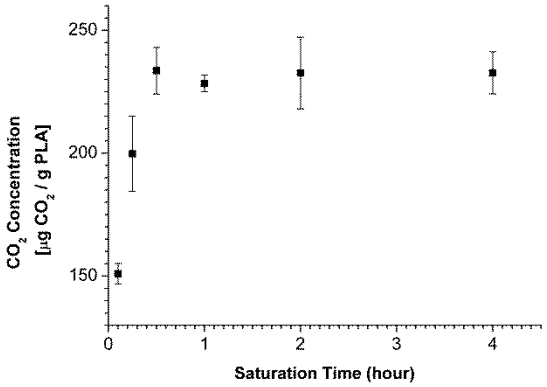

Figure 5.1 CO_2 uptake in neat PLA at room temperature and 1000 psi

Figure 5.2 (a) showed the sorption curve of PLA-hBN_{AC6041} composites with 10 vol.% filler loading. In order to compare the results with neat PLA's sorption study, the CO_2 concentration was normalized with respect to the weight of PLA in the composites, and was illustrated in Figure 5.2 (b). It can be seen that the equilibrium CO_2 concentration in PLA at 1000 psi and room temperature was approximately 240 μg CO_2 per g of PLA (24 wt.%). The results suggested that the addition of hBN_{AC6041} has negligible effect on CO_2's solubility. More importantly, it was found that the CO_2 concentration could reach equilibrium with 1 hour's saturation at 1000 psi. This saturation time and pressure were used in subsequent PLA-hBN_{AC6041} foaming study.

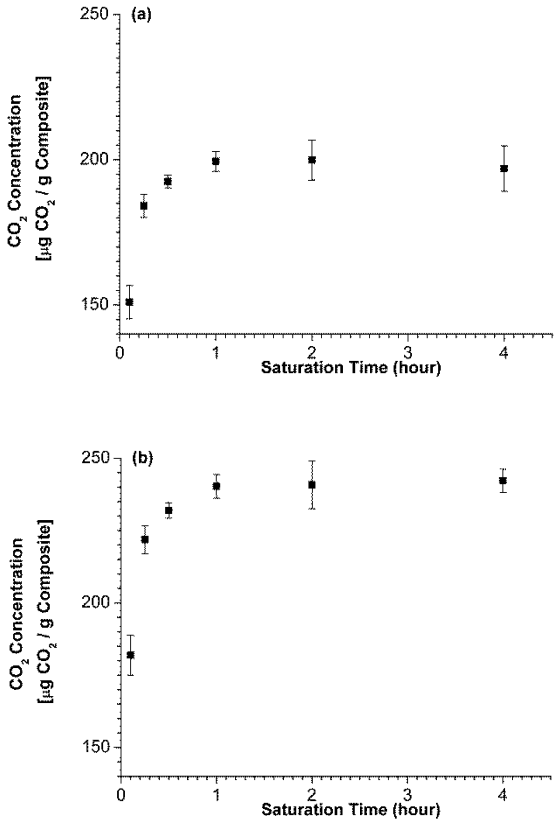

Figure 5.2 (a) CO_2 up take in PLA-hBN_{AC6041} (10 vol.%) at room temperature and 1000 psi; and (b) Normalized CO_2 up take in PLA-hBN_{AC6041} (10 vol.%) at room temperature and 1000 psi

5.2.2 Foaming Study

After the sorption study, a series of foaming studies was carried out for both neat PLA and PLA-hBN_{AC6041} composites. The effect of desorption time, foaming temperature and foaming time was investigated.

5.2.2.1 Foaming Study for Neat PLA

A previous research suggested that a suitable foaming time can maximize the foam's volume expansion [103]. The authors believe that with a short desorption time the gas concentration at the surface region of the samples is still high. It will foam and provide channels

for the gas deep inside to escape without participating in the foaming process. Although this is not a settled conclusion, it is believed this phenomenon is related to the CO_2 concentration at the surface region. In order to determine an appropriate desorption time, a series of foaming studies were conducted by varying desorption time, while maintaining other foaming parameters (foamed at 100 °C for 5 seconds). The effect of desorption time on volume expansion is shown in Figure 5.3. The results suggested that 30 minutes desorption could create largest foam expansion.

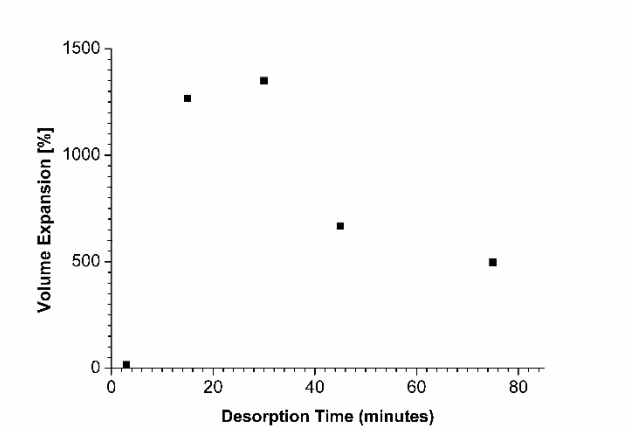

Figure 5.3 Effect of desorption time on foam's volume expansion

In order to compare the foam morphologies, Figure 5.4 presented the SEM micrographs of neat PLA foams with different desorption times. It can be seen that foams obtained with 30 and 45 minutes of desorption time have both larger volume expansion and more uniform cell morphology compared to samples prepared with other desorption times. If the desorption time was shorter that the optimal time, the CO_2 concentration at the surface region would be too high. Figure 5.4 (b) shows that samples with 15-minute desorption time has a thin layer of unfoamed skin. In extreme case (i.e. 3 minutes), the entire sample was not foamed, due to the extremely high CO_2 concentration at the surface. By contrast, excessive desorption time would

allow too much CO_2 to diffuse away through the surface, and the amount of CO_2 participated in the foaming process is insufficient. This would result in a not well foamed sample (Figure 5.4 (e)). The under-foamed surface region in Figure 5.4 (b) and (e) further proved that a suitable CO_2 concentration at the surface region is important to obtain a uniform foam morphology. In order to obtain large volume expansion and uniform foam morphology, 30 minutes desorption time was used for all subsequent foaming studies.

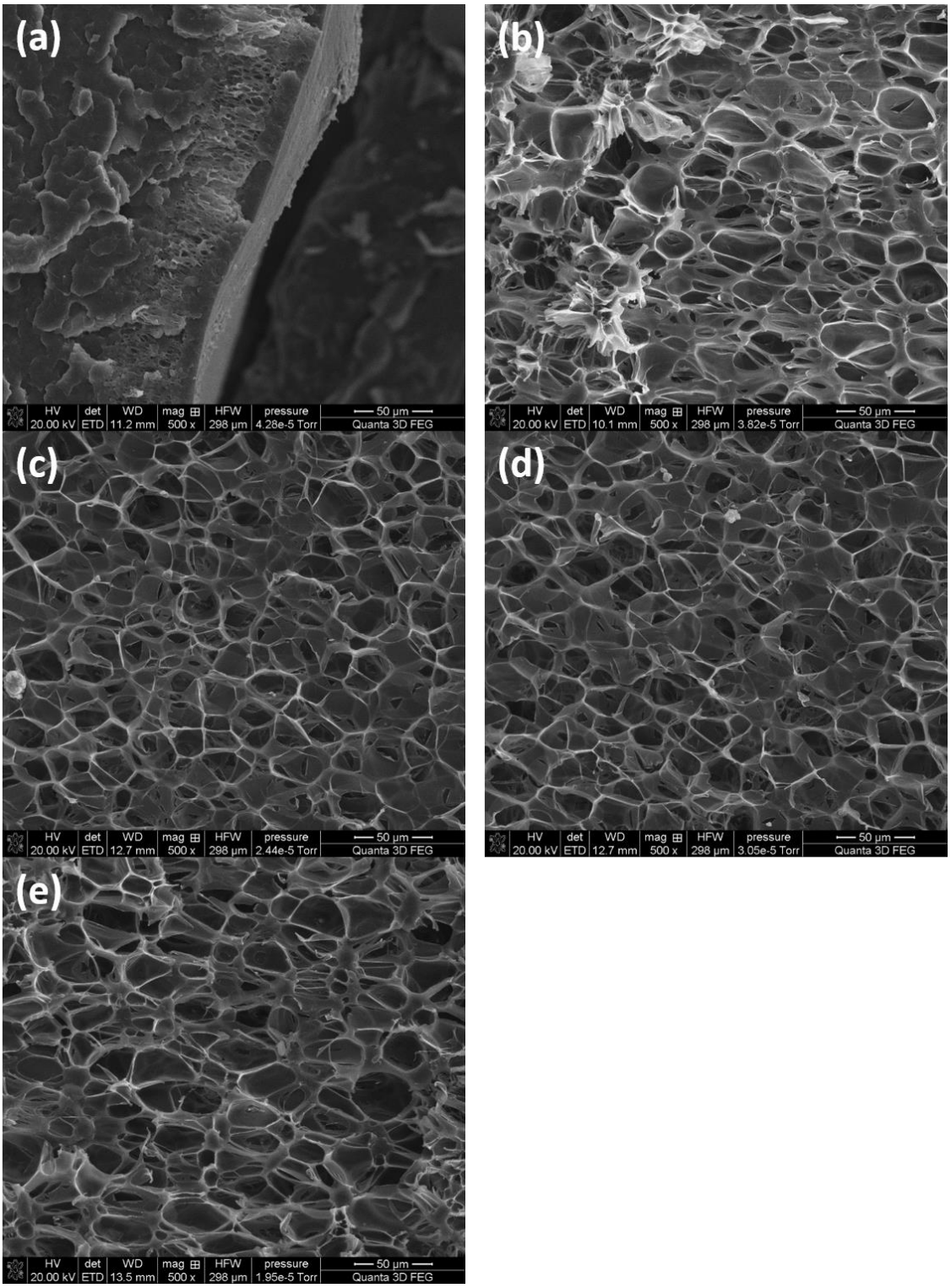

Figure 5.4 SEM images of samples foamed at 100 °C for 5 seconds with different desorption time: (a) 3 minutes desorption; (b) 15 minutes desorption, (c) 30 minutes desorption, (d) 45 minutes desorption; and (e) 60 minutes desorption

5.2.2.2 Foaming Study for PLA-hBN$_{AC6041}$ Composite

The second phase of foaming study investigated how foaming time and foaming temperature affect PLA-hBN$_{AC6041}$ (with 10 vol.% filler loading) composite foams' morphology. Table 5.2 listed all foaming conditions that have been studied. This foaming study provided important information to determine foaming conditions that will be used to fabricate PLA-hBN$_{AC6041}$ composite foams for k_{eff} measurements.

Table 5.2 Foaming conditions studied for PLA-hBN$_{AC6041}$ composite foams

	Foaming Temperature				
	100 °C	**110 °C**	**120 °C**	**130 °C**	**140 °C**
Foaming Time	3 s	3 s	3 s	3 s	3 s
	5 s	5 s	5 s	5 s	5 s
	10 s	10 s	10 s	10 s	10 s
	15 s	15 s	15 s	15 s	15 s
	20 s	20 s	20 s	20 s	20 s

The apparent density of each foamed sample was obtained by weighing the sample both in air and in water. The apparent density was used to calculate the foam's volume expansion with Equation 5.2, and the calculated results were plotted in Figure 5.5. It was found that the volume expansion of samples prepared with excessive foaming time (i.e. > 10 s) are not sensitive to the foaming temperature, and the volume expansions are generally small. For the samples that are prepared with 3 s and 5 s foaming time, the volume expansion has a wide

range; and the values are distributed in this range in a relatively uniform manner. This enabled the fabrication of PLA-hBN_{AC6041} composite foams with different levels of volume expansion, and provided the chance to explore the volume expansion's effect on the k_{eff}.

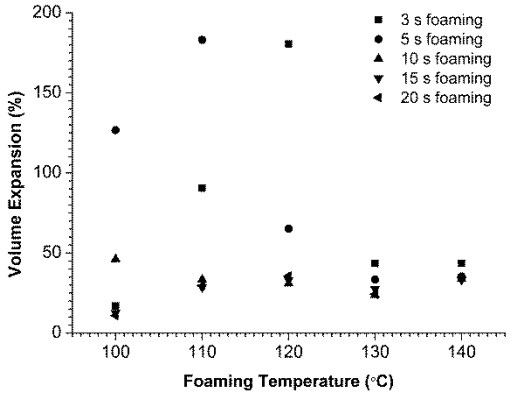

Figure 5.5 Volume expansion % of sample's prepared with different foaming time and temperature.

$$VolumeExpansion = \left(\frac{V_{foam} - V_{solid}}{V_{solid}} \right) \times 100\% = \left(\frac{\rho_{solid}}{\rho_{foam}} - 1 \right) \times 100\% \quad (5.2)$$

where V_{foam} is the volume of the PMC foam sample; V_{solid} is the volume of the solid portion of the sample; ρ_{solid} is the density of unfoamed sample and ρ_{foam} is the apparent density of the composite foam.

5.2.3 k_{eff} of PLA-hBN_{AC6041} Composite Foamed by CO_2

Based on the results of foaming study of PLA-hBN_{AC6041} composite foams (Chapter 5.2.2.2), four conditions were chosen to fabricate PLA-hBN_{AC6041} composites foams for the measurement of their k_{eff}. Table 5.3 summarized the foaming parameters and their corresponding volume expansion. A constant foaming time, 5 seconds, was chosen to provide a wide range of sample's volume expansion. It is noted that the foaming temperature of 140 °C

was not used to prepare samples for the measurement of their k_{eff}, because it generates a volume expansion close to samples foamed at 130 °C (see figure 5.5).

Table 5.3 Foaming conditions and their corresponding volume expansion for PLA-hBN_{AC6041} composite foams

Desorption Time (min.)	Foaming Time (s)	Foaming Temperature (°C)	Volume Expansion (%)
30	5	100	126
30	5	110	183
30	5	120	65
30	5	130	35

The k_{eff} of samples prepared with the aforementioned foaming conditions were measured and reported in Figure 5.6. It was found that the k_{eff} decreased monotonically with respect to volume expansion; and the mound-shaped curves observed in Figure 4.4 and 4.6 were absent. In other words, no foamed sample demonstrated higher k_{eff} than the solid counterpart. One possible reason is that no sample has a volume expansion close to 25%, which is the best case scenario overserved in Chapter 4. The failure of achieving promoted k_{eff} could also be attributed to that one or more of foaming's positive effects on PMC's k_{eff} did not function properly in the samples prepared with solid state foaming.

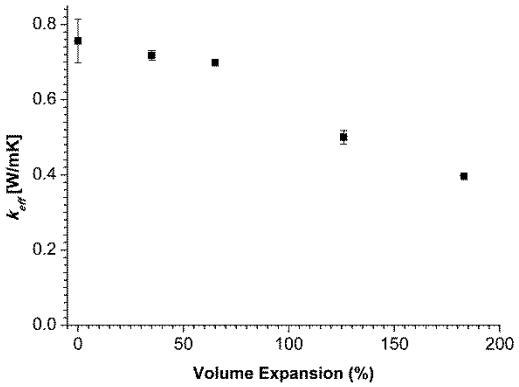

Figure 5.6 Effect of volume expansion on k_{eff} of PLA-hBN$_{AC6041}$ foams blown by CO_2

As discussed in Chapter 4, foaming has two mechanisms that are beneficial for promoting the k_{eff}: 1) increasing effective filler loading by localizing fillers in the solid phase; and 2) aligning fillers along expanding cell walls with foaming-induced biaxial stress field. In order to identify which mechanism(s) failed in the PMC foams prepared with solid state foaming, the foam morphologies of the samples were observed with an SEM microscopy; and the resulting SEM images are presented in Figure 5.7. The cell population densities and cell sizes of samples prepared under each condition are presented in Figure 5.8 and 5.9, respectively. It is found that the cell sizes for all samples are less than 10 µm, which is much smaller compared to that of the samples foamed with Expancel® microspheres (56 µm to 120 µm). The small cell size was not able to effectively align fillers along the cell walls, hence the second mechanism became insignificant, which subsequently failed to enhance the k_{eff} of PMC foams. Although no foamed sample demonstrated k_{eff} higher than the solid counterpart, samples with 35% volume expansion and the solid counterpart have close k_{eff} values (0.72 W/mK and 0.76 W/mK, respectively). In other words, the mass density and material cost were reduced without significantly compromise the k_{eff}.

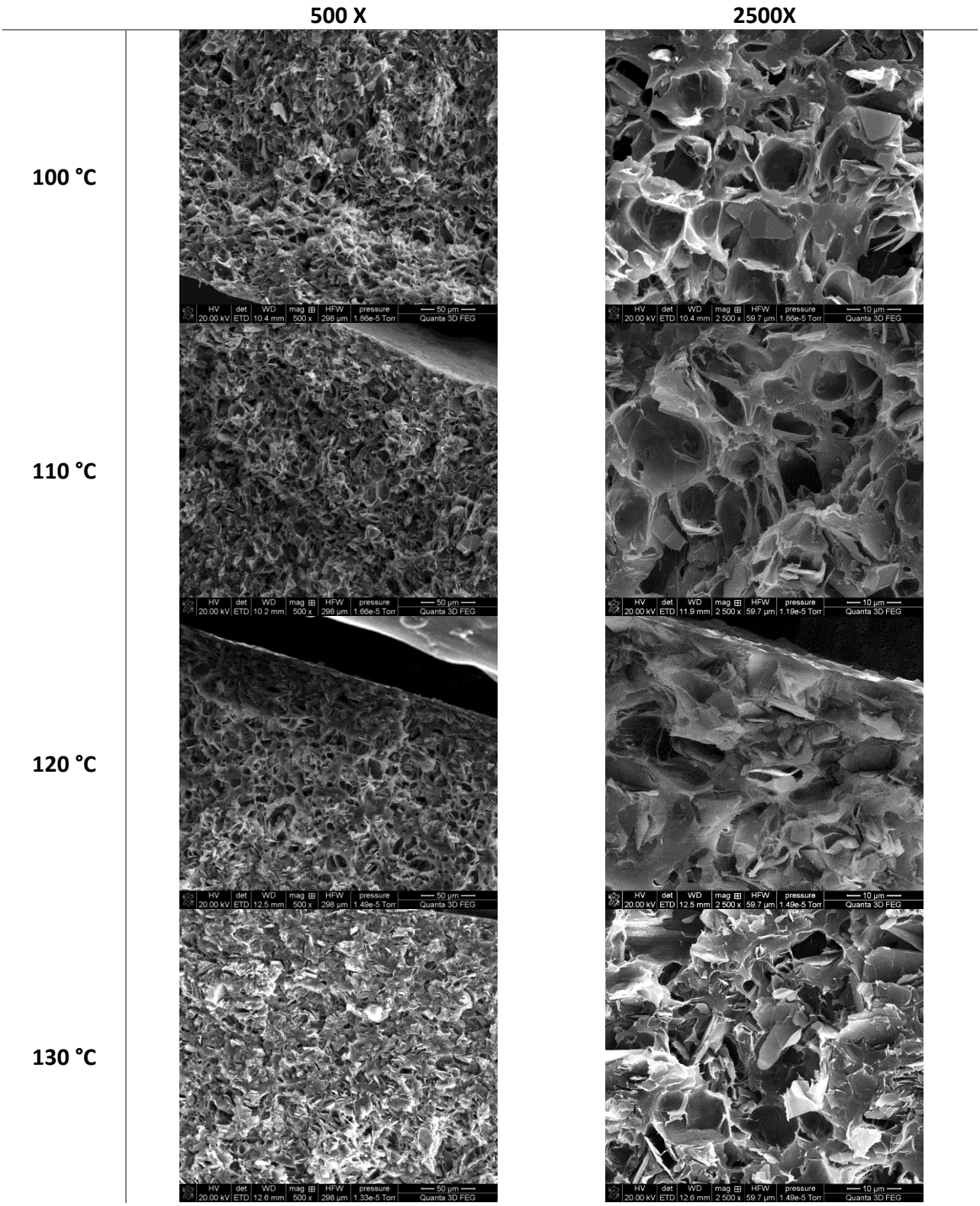

Figure 5.7 EM images of PLA-hBN$_{AC6041}$ composites foams prepared with conditions listed in Table 5.3

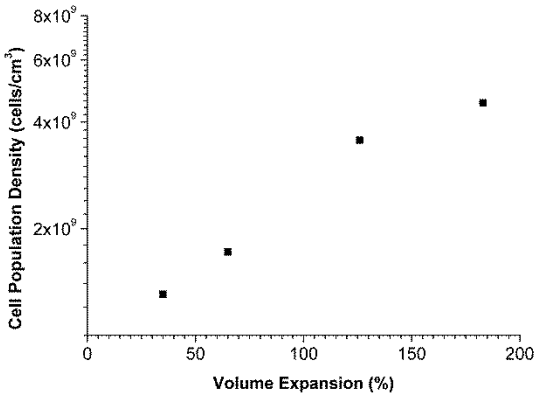

Figure 5.8 Cell population density of PLA-hBN$_{AC6041}$ composites foams with different volume expansion

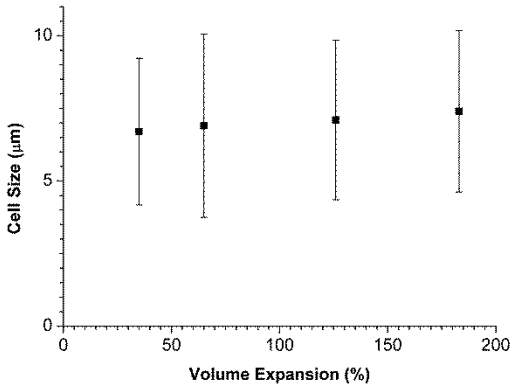

Figure 5.9 Cell size of PLA-hBN$_{AC6041}$ composites foams with different volume expansion

5.3 Conclusion

This study explored the feasibility of producing thermally conductive PMC foams with the method of solid state foaming. PLA-hBN$_{AC6041}$ composites foamed with CO_2 were studied as a case example. First, a series of sorption studies was conducted at 1000 psi for both neat PLA and PLA-hBN$_{AC6041}$ composites to determine the solubility of CO_2 in PLA. It was found that the addition of hBN$_{AC6041}$ does not have a significant effect on CO_2's solubility in PLA. Moreover, the

sorption results suggested that CO_2 uptake in PLA can reach equilibrium within one hour at 1000 psi. This provided a guideline for saturation time in the subsequent foaming study. Secondly, both neat PLA foams and PLA-hBN_{AC6041} composite foams were fabricated using solid state foaming. The effects of desorption time, foaming temperature, and foaming time were studied by setting the other two as controlled variables. It was found that an appropriate desorption time (i.e., 30 minutes to 45 minutes) can generate well expanded foam with uniform cell morphologies. Finally, the k_{eff} were measured for selected foaming conditions as well as the solid counterparts with same filler loading. Although no foamed samples demonstrated k_{eff} higher than the solid counterpart, the k_{eff} of samples with 35% volume expansion (0.72 W/mK) was found to be close to the solid counterpart (0.76 W/mK). In other words, the mass density and material cost were reduced without significantly compromise the k_{eff}. The failure to reach enhanced k_{eff} was believed to be caused by the small cell size, which was not able to effectively align fillers along the cell walls. Once the cell size can be increased by varying foaming parameters (e.g., rate of depressurization), it is anticipated that the same results as Expancel® blown PMC foams can be obtained, and the k_{eff} can be improved.

Chapter 6

Conclusion and Recommendations

6.1 Contribution

The miniaturization of electronic devices is hinged to effective heat dissipation. This requires new multifunctional materials with high thermal conductivity and good electrical resistivity. Owing to their good electrical insulation, light weight, low cost and good processability, polymer based materials have been widely used as packaging materials in the electronics industry. With enhanced thermal conductivity, the heat dissipation rate can be greatly increased. Furthermore, thermally conductive PMCs has the potential to replace traditional metallic heat sinks. In this context, this thesis aims to develop a thermally conductive polymer material system. More specifically, this thesis utilized foaming-induced filler localization and alignment to promote the formation of thermally conductive filler network. Foaming can localize filler particles in the solid phase, hence increase the chance of filler interconnection. Moreover, the foaming-induced biaxial stress field can align thermally conductive filler along expanding cell walls, which can further increase the possibility of filler connection. The well-developed filler interconnection can form a conductive filler network, which can reduce phonon scattering during heat transfer and increase the k_{eff}.

First, an analytical model was developed to confirm the feasibility of foaming-induced k_{eff} enhancement. After being verified with existing experimental data, parametric studies were

conducted to investigate the effects of foam morphology and filler's anisotropic thermal conductivity on the PMC foam's k_{eff}. It was found that constrained foaming to promote expansion in the heat flow direction would enhance the PMC foam's k_{eff}. Moreover, the effectiveness of using foaming as a fabrication strategy to promote PMC's k_{eff} would increase with the anisotropy of filler's thermal conductivity. These findings provided new insights to design thermally conductive PMC foams and guidelines for subsequent experimental studies.

Second, an extensive experimental study was conducted. LDPE-hBN composites blown by Expancel® microspheres were studied as a case example to prove the concept. The results parametrically revealed the structure-to-property relationship of thermally conductive PMC foams. It was found that there exists an optimal foam volume expansion and cell size that can maximize the PMC foam's k_{eff}. Both foam volume expansion and cell size had competing effects on the PMC foam's k_{eff}. PMC foams with moderate volume expansion can localize fillers in the solid phase, which promoted the hBN platelets' interconnectivity. However, high volume expansion percent would result in high volume fraction of thermally insulating air voids, which is detrimental for the k_{eff}. Likewise, an appropriate cell size can maximize the PMC foam's k_{eff}. The initial cell expansion would create a biaxial stress field that align fillers along the cell walls, and promoted the PMC foam's k_{eff}. Nevertheless, excessive cell expansion could disrupt the development of interconnected filler network, and subsequently suppress the PMC foam's k_{eff}. More importantly, this study represented the first time that a PMC foam has a k_{eff} higher than the solid counterpart with same filler loading.

Finally, physical foaming was studied as the fabrication method to produce thermally conductive PMC foams. Compared to Expancel® Microspheres, physical foaming is a more feasible way in larger scale production. The study used CO_2 as physical blowing agent, PLA as polymer matrix, and hBN_{AC6041} as thermally conductive filler. Although no foamed samples that are more thermally conductive than the solid counterpart has been achieved, this study reported PMC foams with reduced mass density and material cost without significantly scarifying its k_{eff}.

6.2 Recommendation for Future Work

This thesis research focused on utilizing foaming to promote filler interconnection, hence improve the k_{eff} of the polymer material system. While this thesis work has demonstrated foaming can promote the formation of thermally conductive network, it is important to further reduce the phonon scattering by minimizing the contact resistance between filler-filler surface and filler-polymer surface. It is recommended to investigate surface treatment methods (e.g. surface coating and functionalization) that can improve the filler-polymer compatibility.

In the last study, physically foamed samples was not able to achieve k_{eff} higher than their solid counterparts. This is believed to be caused by the small cell size, which failed to effectively align fillers along the cell wall. It is recommended to investigate the foaming parameters to obtain PMC foams with larger cell size. This may involve using different saturation pressures, pressure drop rates, foaming time and foaming temperature in the foaming process.

Finally, this thesis study only focused on the k_{eff} of the material system. There are still some other material properties that should be evaluated in future studies before using such thermally conductive PMC foams in electronic packaging or other applications. These properties include, but not limited to, tensile strength, coefficient of thermal expansion, and dielectric properties.

Bibliography

[1]. Mack, C. (2011). Fifty years of Moore's law. *Semiconductor Manufacturing, IEEE Transactions on*, *24*(2), 202-207.

[2]. Beanato, G., Giovannini, P., Cevrero, A., Athanasopoulos, P., Zervas, M., Temiz, Y., & Leblebici, Y. (2012). Design and testing strategies for modular 3-D-multiprocessor systems using die-level through silicon via technology.*Emerging and Selected Topics in Circuits and Systems, IEEE Journal on*, *2*(2), 295-306.

[3]. Yung, K. C., Wang, J., & Yue, T. M. (2008). Thermal management for boron nitride filled metal core printed circuit board. *Journal of Composite Materials*, *42 (24), 2615-2627*

[4]. Lee, G. W., Park, M., Kim, J., Lee, J. I., & Yoon, H. G. (2006). Enhanced thermal conductivity of polymer composites filled with hybrid filler. *Composites Part A: Applied science and manufacturing*, *37*(5), 727-734.

[5]. Dupont. (2010). Kapton data sheet.

[6]. Asai, H., Yano, K. I., Iyogi, K., Iwase, N., & Fujiwara, T. (1999). Design and characteristics of a newly developed cavity-up plastic and ceramic laminated thin BGA package. *Advanced Packaging, IEEE Transactions on*, *22*(3), 460-467.

[7]. Nishino, T., Kotera, M., & Sugiura, Y. (2009). Residual stress of particulate polymer composites with reduced thermal expansion. In *Journal of Physics: Conference Series* (Vol. 184, No. 1, p. 012026). IOP Publishing.

[8]. Manzione, L. T. (1990). *Plastic packaging of microelectronic devices*. Van Nostrand Reinhold.

[9]. Mamunya, Y. P., Davydenko, V. V., Pissis, P., & Lebedev, E. V. (2002). Electrical and thermal conductivity of polymers filled with metal powders.*European polymer journal*, *38*(9), 1887-1897.

[10]. Tekce, H. S., Kumlutas, D., & Tavman, I. H. (2007). Effect of particle shape on thermal conductivity of copper reinforced polymer composites. *Journal of Reinforced Plastics and Composites*, *26*(1), 113-121.

[11]. Yung, K. C., & Liem, H. (2007). Enhanced thermal conductivity of boron nitride epoxy-matrix composite through multi-modal particle size mixing. *Journal of Applied Polymer Science*, *106*(6), 3587-3591.

[12]. Leung, S. N., Khan, M. O., Chan, E., Naguib, H. E., Dawson, F., Adinkrah, V., & Lakatos-Hayward, L. (2013). Synergistic effects of hybrid fillers on the development of thermally conductive polyphenylene sulfide composites. *Journal of Applied Polymer Science*, *127*(5), 3293-3301.

[13]. King, J. A., Johnson, B. A., Via, M. D., & Ciarkowski, C. J. (2010). Effects of carbon fillers in thermally conductive polypropylene based resins. *Polymer Composites*, *31*(3), 497-506.

[14]. Tu, H., & Ye, L. (2010). Preparation and characterization of thermally conductive polystyrene/carbon nanotubes composites. *Journal of applied polymer science*, *116*(4), 2336-2342.

[15]. Wattanakul, K., Manuspiya, H., & Yanumet, N. (2011). Thermal conductivity and mechanical properties of BN-filled epoxy composite: effects of filler content, mixing conditions and BN agglomerate size. *Journal of Composite Materials*, 0021998310393297.

[16]. Zhou, W. Y., Qi, S. H., Zhao, H. Z., & Liu, N. L. (2007). Thermally conductive silicone rubber reinforced with boron nitride particle. *Polymer composites*, *28*(1), 23-28.

[17]. Chung, S., Im, Y., Kim, H., Park, S., & Jeong, H. (2005). Evaluation for micro scale structures fabricated using epoxy-aluminum particle composite and its application. *Journal of materials processing technology*, *160*(2), 168-173.

[18]. Chan, E., Leung, S. N., Khan, M. O., Naguib, H. E., Dawson, F., & Adinkrah, V. (2012). Novel Thermally Conductive Thermoplastic/Ceramic Composite Foams. *Macromolecular Materials and Engineering*, *297*(10), 1014-1020.

[19]. Smagorinski, M. E., Tsantrizos, P. G., Grenier, S., Cavasin, A., Brzezinski, T., & Kim, G. (1998). The properties and microstructure of Al-based composites reinforced with ceramic particles. *Materials Science and Engineering: A*, *244*(1), 86-90.

[20]. Yunus, A. C. (2003). Heat transfer: a practical approach. *MacGraw Hill, New York*.

[21]. Tsutsumi, N.; Takeuchi, N.; Kiyotsukuri, T. J. Polym. Sci., Part B: Polym. Phys. 1991, 29, 1085-1093.

[22]. Parrott, J. E., & Stuckes, A. D. (1975). *Thermal conductivity of solids*. Pion Limited.

[23]. Berman, R. (1976). Thermal conductivity in solids. *Clarendon, Oxford*.

[24]. Bigg, D. M. (1986). Thermally conductive polymer compositions. *Polymer composites*, *7*(3), 125-140.

[25]. Hauser, R. A. (2008). *Synergistic effects and modeling of thermally conductive resins for fuel cell bipolar plate applications*. ProQuest.

[26]. Callister, W. D., & Rethwisch, D. G. (2012). *Fundamentals of materials science and engineering: an integrated approach*. John Wiley & Sons.

[27]. Henry, A., Chen, G., Plimpton, S. J., & Thompson, A. (2010). 1D-to-3D transition of phonon heat conduction in polyethylene using molecular dynamics simulations. *Physical Review B*, *82*(14), 144308.

[28]. Shen, S., Henry, A., Tong, J., Zheng, R., & Chen, G. (2010). Polyethylene nanofibres with very high thermal conductivities. *Nature nanotechnology*, *5*(4), 251-255.

[29]. Shindé, S. L., & Goela, J. (2006). *High thermal conductivity materials*. New York: Springer.

[30]. Chiang, Y. M., Kingery, W. D., & Birnie, D. P. (1997). *Physical ceramics: principles for ceramic science and engineering*. J. Wiley.

[31]. Watari*,* K., & Shinde, S. L. *(2001).* High thermal conductivity materials*. MRS Bulletin, 26(06), 440-444.*

[32]. Mazumdar, S. (2001). *Composites manufacturing: materials, product, and process engineering*. CrC press.

[33]. GE Engineering Thermoplastic Product Guide: Material Selection. GE Plastics.

[34]. M. P. Stevens, Polymer Chemistry: An Introduction. Oxford University Press, New York, 1999

[35]. Wool, R. P. (1993). Polymer entanglements. Macromolecules, 26(7), 1564-1569.

[36]. Hansen, D., & Bernier, G. A. (1972). Thermal conductivity of polyethylene: the effects of crystal size, density and orientation on the thermal conductivity.*Polymer Engineering & Science*, 12(3), 204-208.

[37]. Piraux, L., Ducarme, E., Issi, J. P., Begin, D., & Billaud, D. (1991). Thermal conductivity of oriented polyacetylene films. Synthetic Metals, 41(1), 129-132.

[38]. Sundstrom, D. W., & Lee, Y. D. (1972). Thermal conductivity of polymers filled with particulate solids. Journal of Applied Polymer Science, 16(12), 3159-3167.

[39]. Fried, J. R. Polymer Science and Technology. Prentice Hall, New Jersey, 1995.

[40]. Watari, Koji, Mitsuru Kawamoto, and Kozo Ishizaki. "Sintering chemical reactions to increase thermal conductivity of aluminium nitride." *Journal of materials science* 26, no. 17 (1991): 4727-4732.

[41]. Raman, Chandrashekar, and Paulo Meneghetti. "Boron nitride finds new applications in thermoplastic compounds." *Plastics, Additives and Compounding* 10, no. 3 (2008): 26-31.

[42]. Bridgwater, J. (1976). Fundamental powder mixing mechanisms. *Powder Technology*, *15*(2), 215-236.

[43]. Chae, D. W., & Kim, B. C. (2005). Characterization on polystyrene/zinc oxide nanocomposites prepared from solution mixing. *Polymers for advanced technologies*, *16*(11-12), 846-850.

[44]. Rosca, I. D., & Hoa, S. V. (2009). Highly conductive multiwall carbon nanotube and epoxy composites produced by three-roll milling. *Carbon*, *47*(8), 1958-1968.

[45]. Lin, B., Sundararaj, U., & Pötschke, P. (2006). Melt Mixing of Polycarbonate with Multi-Walled Carbon Nanotubes in Miniature Mixers. *Macromolecular Materials and Engineering*, *291*(3), 227-238.

[46]. Park, C., Ounaies, Z., Watson, K. A., Crooks, R. E., Smith, J., Lowther, S. E., Connell, J. W., Siochi, E. J., Harrison, J. S., & St Clair, T. L. (2002). Dispersion of single wall carbon nanotubes by in situ polymerization under sonication. *Chemical physics letters*, *364*(3), 303-308.

[47]. Agari, Y., Ueda, A., & Nagai, S. (1991). Thermal conductivities of composites in several types of dispersion systems. Journal of Applied Polymer Science,42(6), 1665-1669.

[48]. Lee, S. M. Epoxy Resin, Marcel Deker Inc., New York, 1988

[49]. Gross, K., S. Hackett, D. Larkey, W. Schultz, W. Thompson. Proceedings of the international symposium on microelectronics, Denver, CO. (September 2002) p. 234–238.

[50]. Sun. Y., C.P. Wong. Proceedings of the 54th electronic components and technology conference, Las Vegas, NV (June 2004) p. 477–483.

[51]. Lee, Eun-Sung, Sang-Mock Lee, Daniel J. Shanefield, and W. Roger Cannon. "Enhanced thermal conductivity of polymer matrix composite via high solids loading of aluminum nitride in epoxy resin." *Journal of the American Ceramic Society* 91, no. 4 (2008): 1169-1174

[52]. Wong, C. P., and Raja S. Bollampally. "Thermal conductivity, elastic modulus, and coefficient of thermal expansion of polymer composites filled with ceramic particles for electronic packaging." *Journal of Applied Polymer Science* 74, no. 14 (1999): 3396-3403.

[53]. Lee, Bin, and Gance Dai. "Influence of interfacial modification on the thermal conductivity of polymer composites." *Journal of materials science* 44, no. 18 (2009): 4848-4855.

[54]. Yung, K. C., and H. Liem. "Enhanced thermal conductivity of boron nitride epoxy-matrix composite through multi-modal particle size mixing." *Journal of Applied Polymer Science* 106, no. 6 (2007): 3587-3591.

[55]. Huang, X., Liu, W., Jiang, P., & Tanaka, T. (2011, September). Boron nitride based poly (phenylene sulfide) compsoites with enhanced thermal conductivity and breakdown strength. In *Electrical Insulating Materials (ISEIM), Proceedings of 2011 International Conference on* (pp. 35-38). IEEE.

[56]. Haggenmueller, R., Guthy, C., Lukes, J. R., Fischer, J. E., & Winey, K. I. (2007). Single wall carbon nanotube/polyethylene nanocomposites: thermal and electrical conductivity. *Macromolecules*, *40*(7), 2417-2421.

[57]. Kalaitzidou, K., Fukushima, H., & Drzal, L. T. (2007). Multifunctional polypropylene composites produced by incorporation of exfoliated graphite nanoplatelets. *Carbon*, *45*(7), 1446-1452.

[58]. Agari, Y., & Uno, T. (1985). Thermal conductivity of polymer filled with carbon materials: effect of conductive particle chains on thermal conductivity. *Journal of applied polymer science*, *30*(5), 2225-2235.

[59]. Martin, C. A., Sandler, J. K. W., Windle, A. H., Schwarz, M. K., Bauhofer, W., Schulte, K., & Shaffer, M. S. P. (2005). Electric field-induced aligned multi-wall carbon nanotube networks in epoxy composites. *Polymer*, *46*(3), 877-886.

[60]. Leung, S. N., Khan, M. O., Naguib, H., & Dawson, F. (2014). Multifunctional polymer nanocomposites with uniaxially aligned liquid crystal polymer fibrils and graphene nanoplatelets. *Applied Physics Letters*, *104*(8), 081904.

[61]. Yu, A., Ramesh, P., Sun, X., Bekyarova, E., Itkis, M. E., & Haddon, R. C. (2008). Enhanced thermal conductivity in a hybrid graphite nanoplatelet–carbon nanotube filler for epoxy composites. *Advanced Materials*, *20*(24), 4740-4744.

[62]. Okamoto, M., Nam, P. H., Maiti, P., Kotaka, T., Nakayama, T., Takada, M., ... & Okamoto, H. (2001). Biaxial flow-induced alignment of silicate layers in polypropylene/clay nanocomposite foam. *Nano letters*, *1*(9), 503-505.

[63]. Li, J., Ma, P. C., Chow, W. S., To, C. K., Tang, B. Z., & Kim, J. K. (2007). Correlations between percolation threshold, dispersion state, and aspect ratio of carbon nanotubes. *Advanced Functional Materials*, *17*(16), 3207-3215.

[64]. Evans, W., Prasher, R., Fish, J., Meakin, P., Phelan, P., & Keblinski, P. (2008). Effect of aggregation and interfacial thermal resistance on thermal conductivity of nanocomposites and colloidal nanofluids. *International Journal of Heat and Mass Transfer*, *51*(5), 1431-1438.

[65]. Kapadia, R. S., Louie, B. M., & Bandaru, P. R. (2014). The influence of carbon nanotube aspect ratio on thermal conductivity enhancement in nanotube–polymer composites. *Journal of Heat Transfer*, *136*(1), 011303.

[66]. R. Kochetov, Thermal and electrical properties of nanocomposites, including material processing, PhD dissertation, Delft University of Technology, 2012.

[67]. Mosanenzadeh, S. G., Khalid, S., Cui, Y., & Naguib, H. E. (2015). High thermally conductive PLA based composites with tailored hybrid network of hexagonal boron nitride and graphene nanoplatelets. *Polymer Composites*.

[68]. Weidenfeller, B., Höfer, M., & Schilling, F. R. (2004). Thermal conductivity, thermal diffusivity, and specific heat capacity of particle filled polypropylene.*Composites Part A: applied science and manufacturing*, *35*(4), 423-429.

[69]. Choudhury, M., Mohanty, S., Nayak, S. K., & Aphale, R. (2012). Preparation and characterization of electrically and thermally conductive polymeric nanocomposites. *Journal of Minerals and Materials Characterization and Engineering*, *11*(07), 744.

[70]. Irwin, P. C., Cao, Y., Bansal, A., & Schadler, L. S. (2003, October). Thermal and mechanical properties of polyimide nanocomposites. In *Electrical Insulation and Dielectric Phenomena, 2003. Annual Report. Conference on* (pp. 120-123). IEEE.

[71]. Rong, M. Z., Zhang, M. Q., & Ruan, W. H. (2006). Surface modification of nanoscale fillers for improving properties of polymer nanocomposites: a review. Materials science and technology, 22(7), 787-796.

[72]. Tavman, I. H., & Akinci, H. (2000). Transverse thermal conductivity of fiber reinforced polymer composites. *International Communications in Heat and Mass Transfer*, *27*(2), 253-261.

[73]. McCullough, R. L. (1985). Generalized combining rules for predicting transport properties of composite materials. *Composites Science and Technology*, *22*(1), 3-21.

[74]. Maxwell, J. C. (1881). *A treatise on electricity and magnetism* (Vol. 1). ; Dover: New York. 3rd ed.

[75]. Progelhof, R. C., Throne, J. L., & Ruetsch, R. R. (1976). Methods for predicting the thermal conductivity of composite systems: a review. *Polymer Engineering & Science*, *16*(9), 615-625.

[76]. Bruggeman, D. A. G. (1935). Dielectric constant and conductivity of mixtures of isotropic materials. *Ann Phys (Leipzig)*, *24*, 636-679.

[77]. Agari, Y., & Uno, T. (1986). Estimation on thermal conductivities of filled polymers. Journal of Applied Polymer Science, 32(7), 5705-5712.

[78]. Agari, Y., Ueda, A., & Nagai, S. (1993). Thermal conductivity of a polymer composite. *Journal of Applied Polymer Science*, *49*(9), 1625-1634.

[79]. Lewis, T. B., & Nielsen, L. E. (1970). Dynamic mechanical properties of particulate-filled composites. *Journal of Applied Polymer Science*, *14*(6), 1449-1471.

[80]. Nielsen, L. E., & Lee, B. L. (1972). Dynamic mechanical properties of some polystyrene composites. *Journal of Composite Materials*, *6*(1), 136-146.

[81]. Nielsen, L. E. (1974). The thermal and electrical conductivity of two-phase systems. *Industrial & engineering chemistry fundamentals*, *13*(1), 17-20.

[82]. Pal, R. (2008). On the Lewis–Nielsen model for thermal/electrical conductivity of composites. *Composites Part A: Applied Science and Manufacturing*, *39*(5), 718-726.

[83]. Lee, S. T., & Ramesh, N. S. (Eds.). (2004). *Polymeric foams: mechanisms and materials*. CRC press.

[84]. Park, C. B., Baldwin, D. F., & Suh, N. P. (1995). Effect of the pressure drop rate on cell nucleation in continuous processing of microcellular polymers.*Polymer Engineering & Science*, *35*(5), 432-440.

[85]. Eaves, D. (2004). Handbook of polymer foams. *polimeri*, *25*, 1-2.

[86]. Secretariat, O. (2000). The Montreal protocol on substances that deplete the ozone layer. *United Nations Environment Programme, Nairobi, Kenya*.

[87]. Jachtenfuchs, M. (1990). The European Community and the protection of the ozone layer. *JCMS: Journal of Common Market Studies*, *28*(3), 261-277.

[88]. Akzonobel (2014). Expancel® Data Sheet.

[89]. Arjmand, M., Mahmoodi, M., Park, S., & Sundararaj, U. (2014). Impact of foaming on the broadband dielectric properties of multi-walled carbon nanotube/polystyrene composites. *Journal of Cellular Plastics*, *50*(6), 551-562.

[90]. Ameli, A., Nofar, M., Park, C. B., Pötschke, P., & Rizvi, G. (2014). Polypropylene/carbon nanotube nano/microcellular structures with high dielectric permittivity, low dielectric loss, and low percolation threshold. *Carbon*,*71*, 206-217.

[91]. Engler, M., Uibel, K., & Eichler, J. (2010). *U.S. Patent Application 12/964,195*.

[92]. Wang, C., Ying, S., & Xiao, Z. (2013). Preparation of short carbon fiber/polypropylene fine-celled foams in supercritical CO2. *Journal of Cellular Plastics*, *49*(1), 65-82.

[93]. Tanimoto, M., Yamagata, T., Miyata, K., & Ando, S. (2013). Anisotropic thermal diffusivity of hexagonal boron nitride-filled polyimide films: effects of filler particle size, aggregation, orientation, and polymer chain rigidity. *ACS applied materials & interfaces*, *5*(10), 4374-4382.

[94]. NOVA Chemicals (2015). LA-0219-A Data Sheet.

[95]. Leung, S. N., Ghaffari, S., & Naguib, H. E. (2013, April). Development of novel multifunctional biobased polymer composites with tailored conductive network of micro-and-nano-fillers. In *SPIE Smart Structures and Materials+ Nondestructive Evaluation and Health Monitoring* (pp. 86890F-86890F). International Society for Optics and Photonics.

[96]. ASTM International (2004). ASM E1225-04.

[97]. Scherrer, P. (1918). Estimation of the size and internal structure of colloidal particles by means of röntgen. *Nachr. Ges. Wiss. Göttingen*, *2*, 96-100.

[98]. Murray, K. A., Kennedy, J. E., McEvoy, B., Vrain, O., Ryan, D., Cowman, R., & Higginbotham, C. L. (2013). Effects of gamma ray and electron beam irradiation on the mechanical, thermal, structural and physicochemical properties of poly (ether-block-amide) thermoplastic elastomers. *journal of the mechanical behavior of biomedical materials*, *17*, 252-268.

[99]. Wong, A., Guo, Y., & Park, C. B. (2013). Fundamental mechanisms of cell nucleation in polypropylene foaming with supercritical carbon dioxide—Effects of extensional stresses and crystals. *The Journal of Supercritical Fluids*, *79*, 142-151.

[100]. Kai, W., He, Y., & Inoue, Y. (2005). Fast crystallization of poly (3-hydroxybutyrate) and poly (3-hydroxybutyrate-co-3-hydroxyvalerate) with talc and boron nitride as nucleating agents. *Polymer international*, *54*(5), 780-789.

[101]. Li, L. H., Glushenkov, A. M., Hait, S. K., Hodgson, P., & Chen, Y. (2014). High-Efficient Production of Boron Nitride Nanosheets via an Optimized Ball Milling Process for Lubrication in Oil. *Scientific reports*, *4*.

[102]. NatureWorks. (2015) Ingeo™ Biopolymer 8052D Technical Data Sheet

[103]. Wang, X., Li, W., & Kumar, V. (2006). A method for solvent-free fabrication of porous polymer using solid-state foaming and ultrasound for tissue engineering applications. *Biomaterials*, *27*(9), 1924-1929.D

[104]. Matuana, L. M. (2008). Solid state microcellular foamed poly (lactic acid): morphology and property characterization. *Bioresource technology*, *99*(9), 3643-3650.

[105]. ASTM International (2008). ASTM D1622-08.

[106]. ASTM International (2006). ASTM D5470-06.